

# Oxidation of a Levitated 1-Butyl-3-methylimidazolium Dicyanoborate Droplet by Nitrogen Dioxide

Michael Lucas,<sup>†</sup> Stephen J. Brotton,<sup>†</sup> Jan A. P. Sprenger,<sup>‡</sup> Maik Finze,<sup>‡</sup> Shiv K. Sharma,<sup>§</sup> and Ralf I. Kaiser<sup>\*,†</sup>

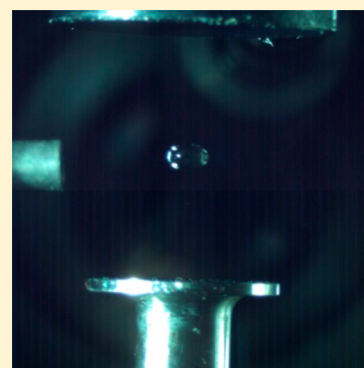
<sup>†</sup>Department of Chemistry, University of Hawaii at Manoa, Honolulu, Hawaii 96822, United States

<sup>‡</sup>Institute for Inorganic Chemistry, Institute for Sustainable Chemistry & Catalysis with Boron (ICB), Julius-Maximilians-Universität Würzburg, Am Hubland, 97074 Würzburg, Germany

<sup>§</sup>Hawaii Institute of Geophysics and Planetology, University of Hawaii at Manoa, Honolulu, Hawaii 96822, United States

## S Supporting Information

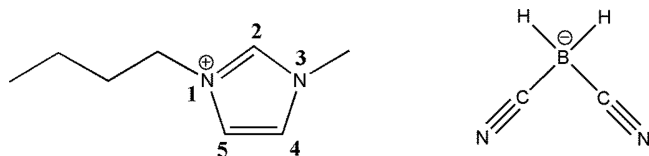
**ABSTRACT:** To develop the next generation of hypergolic, ionic-liquid-based fuels, it is important to understand the fundamental reaction mechanisms for the oxidation of ionic liquids (ILs). We consequently studied the oxidation of a levitated 1-butyl-3-methylimidazolium dicyanoborate ([BMIM][DCBH]) droplet by nitrogen dioxide (NO<sub>2</sub>). The properties of [BMIM][DCBH], including short ignition-delay times, low viscosities, and a wide liquid temperature range, make the ionic liquid especially suitable as a component of a hypergolic fuel. The chemical modifications were monitored with Fourier-transform infrared (FTIR), Raman, and ultraviolet–visible spectroscopies. To identify changes induced by the oxidation, it was first necessary to assign vibrational modes to the FTIR and Raman spectra of unreacted [BMIM][DCBH]. The new features in the oxidized FTIR and Raman spectra could then be identified and assigned on the basis of the possible functional groups likely to form through addition with a nitrogen and an oxygen atom of nitrogen dioxide creating a new bond with the ionic liquid. The assignments suggest that organic nitro-compounds and boron–nitrogen and boron–oxygen containing compounds were produced. A large decrease in the intensity of some [DCBH]<sup>−</sup> fundamental modes suggests the nitrogen dioxide molecule prefers to react with the anion over the cation.



## 1. INTRODUCTION

Liquid bipropellant systems represent one of the most common propulsion methods for rockets.<sup>1</sup> Bipropellant systems involve

### Scheme 1. Molecular Structure of [BMIM][DCBH]<sup>a</sup>



<sup>a</sup>The numbering convention for the position of the atoms in the imidazolium ring is shown.

two chemicals, a fuel and an oxidizer, which spontaneously ignite upon mixing. The ability to spontaneously ignite upon the contact of a fuel with an oxidizer is known as hypergolicity.<sup>1</sup> The exploitation of bipropellants allows for a simple fuel system as only three chambers are necessary: two separate storage chambers for the fuel and the oxidizer, and a third chamber used for mixing when ignition is desired. Because ignition occurs upon contact, there is no need for an external ignition source. The current standard for bipropellant fuels consists of hydrazine (N<sub>2</sub>H<sub>4</sub>) and its methylated derivatives as the fuel and oxidizers

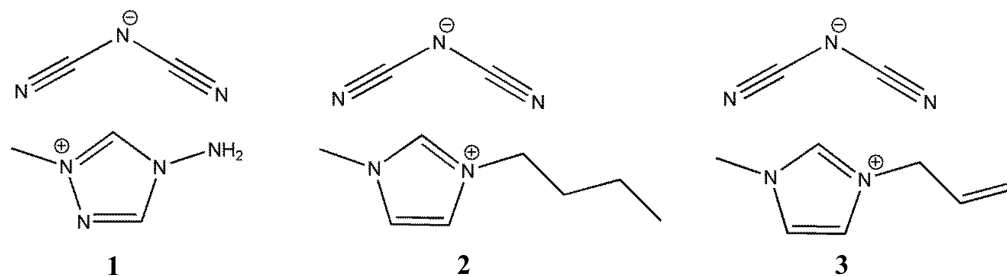
such as white fuming nitric acid (HNO<sub>3</sub>; WFNA), dinitrogen tetroxide in equilibrium with nitrogen dioxide (N<sub>2</sub>O<sub>4</sub> ⇌ 2NO<sub>2</sub>), and hydrogen peroxide (H<sub>2</sub>O<sub>2</sub>).<sup>1</sup> Despite their common use, these fuels possess severe disadvantages. Hydrazine and its derivatives are extremely toxic, carcinogenic, highly volatile, and flammable; this leads to significant handling and storage costs.<sup>2</sup> One of the avenues explored for the next generation of alternative rocket fuels involves energetic ionic liquids (EILs).<sup>2–10</sup> Ionic liquids (ILs) are defined as liquid salts with melting points below 100 °C and generally consist of a large asymmetric, organic cation and an inorganic or organic anion.<sup>2</sup> To be employed as a propellant fuel, the ionic liquid must be hypergolic, be thermally and water stable, have a low viscosity and hence reduced ignition time, and possess low ignition delays (IDs).<sup>8</sup> One of the first EILs found to be hypergolic with WFNA and meeting these criteria consists of an imidazolium-based cation and a dicyanamide ([DCA]<sup>−</sup>) anion.<sup>7,10–13</sup>

Multiple approaches can enhance the energy density of EILs and thus improve their potential as the next generation of rocket fuels. One method is to increase the number of nitrogen–nitrogen bonds by creating ions with more nitrogen atoms, for

Received: December 7, 2018

Published: January 1, 2019

Scheme 2. Molecular Structure of [MAT][DCA] (1), [BMIM][DCA] (2), and [AMIM][DCA] (3)



example, changing the cation from an imidazolium ring to a triazolium ring (Scheme 1).<sup>14,15</sup> The addition of an energetic material to the ionic liquid such as boron, aluminum, or magnesium is an alternative approach. Boron is promising as a potential additive because it has a high volumetric energy density of  $138 \text{ kJ cm}^{-3}$ ;<sup>16</sup> this energy density is higher than for traditional hydrocarbon fuels ( $35\text{--}40 \text{ kJ cm}^{-3}$ ), aluminum ( $84 \text{ kJ cm}^{-3}$ ), or magnesium ( $43 \text{ kJ cm}^{-3}$ ).<sup>16</sup> Despite the potential of boron, severe limitations occurring during the combustion of boron prevent the full energy release. The first issue is a consequence of a boron oxide ( $\text{B}_2\text{O}_3$ ) layer forming on the surface which delays the ignition.<sup>17</sup> Second, the formation of metaboric acid (HOB) in the presence of hydrogen-containing gases creates an “energy trap” or “thermodynamical sink” because a significant fraction of the boron is not converted to boron oxide ( $\text{B}_2\text{O}_3$ ).<sup>17</sup> The boron combustion reactions occur predominantly on the surface and, hence, are limited by the diffusion to and from the surface.<sup>18–21</sup> Anderson *et al.* synthesized hydrogen-loaded boron nanoparticles capped with a suitable IL as a route to help mitigate these limitations.<sup>22–25</sup> The nanoparticles increase the surface-area-to-volume ratio and thus minimize the diffusion limitation. Furthermore, the IL capping of the nanoparticles stabilizes the boron in air by preventing the formation of the boron oxide ( $\text{B}_2\text{O}_3$ ) layer. In related studies, McCrary *et al.* capped boron nanoparticles with 1-methyl-4-amino-1,2,4-triazolium dicyanamide ([MAT][DCA]) or 1-butyl-3-methylimidazolium dicyanamide ([BMIM][DCA]). Ionic liquids containing these IL capped boron nanoparticles when reacted with WFNA were found to retain their hypergolic properties. The addition of the boron nanoparticles improved the burn flame, but the ID was not reduced.<sup>26</sup> Yu *et al.* added borane-aluminum ( $\text{BH}_3\text{--Al}$ ) nanoparticles to hypergolic ILs and also found little change in the ID, but a noticeable increase in the flame size was produced.<sup>27</sup> Our group studied the effect on the oxidation by  $\text{NO}_2$  produced by adding IL-capped boron nanoparticles to three EILs, namely, [MAT][DCA], [BMIM][DCA], and 1-allyl-3-methylimidazolium dicyanamide ([AMIM][DCA]).<sup>28,29</sup> Only the [BMIM][DCA] showed any new spectroscopic features produced by oxidation of the boron, and these were minor, which is consistent with the [BMIM][DCA] capping limiting the oxidation of the nanoparticles. Furthermore, the addition of the boron nanoparticles caused the reaction rate for the oxidation of [BMIM][DCA] to decrease by a factor of approximately 2, which is likely caused by the increased viscosity of the droplet accompanying suspension of the small boron particles.<sup>29</sup>

Incorporating boron into the anion of the IL is an alternative strategy to improve the performance of hypergolic EILs. One of most important properties is possessing a high energy density, which can be found in ILs with large positive heat of formation. Boron-containing anions generally have a larger heat of

formation than other anions such as nitrate ( $\text{NO}_3^-$ ), dicyanamide ([DCA]<sup>-</sup>), and nitrocyanamide ([NCA]<sup>-</sup>).<sup>5,30</sup> To this end, Zhang *et al.* synthesized a series of hypergolic ILs with boron-containing anions.<sup>31</sup> More specifically, [BMIM]<sup>+</sup>-containing ILs incorporating borohydride ( $[\text{BH}_4]^-$ ), cyanoborate ( $[\text{BH}_3\text{CN}]^-$ ), or dicyanoborate ( $[\text{BH}_2(\text{CN})_2]^-$  or [DCBH]<sup>-</sup>) anions were synthesized and shown to be hypergolic with WFNA. The borohydride- and cyanoborate-based ionic liquids are hydrolytically unstable and require anhydrous conditions for preparation and storage.<sup>3,4,9,31</sup> In contrast, [DCBH]<sup>-</sup> is hydrolytically stable and can be synthesized in water, which makes [DCBH]<sup>-</sup>-based ionic liquids ideal candidates for use as a fuel owing to the consequent ease of preparation and storage. Further desirable properties that ionic liquids require for use in bipropellant fuels include a wide liquid temperature range and low melting points, so that the fuel remains liquid across a wide range of temperatures; a low viscosity to allow for the fuel to be easily mixed with the oxidizer; and short ID times.<sup>3,9</sup> [DCBH]<sup>-</sup>-based ionic liquids have been shown to have lower viscosities and shorter ID times, while maintaining a low melting point and wide liquid temperature range compared to ionic liquids containing dicyanamide [DCA]<sup>-</sup> and [NCA]<sup>-</sup> anions, and are thus of especial interest as components of hypergolic fuels.<sup>3,4,9,32</sup>

Here, we explore experimentally the oxidation of levitated 1-butyl-3-imidazolium dicyanoborate ([BMIM][DCBH]; Scheme 2) droplets by nitrogen dioxide ( $\text{NO}_2$ ) using infrared (IR), Raman, and ultraviolet–visible (UV–vis) spectroscopies. We first assign vibrational modes to the pure [BMIM][DCBH] before reaction as a reference to help identify changes in the spectra caused by the reaction with nitrogen dioxide. Second, the key intermediates and functional groups formed by the oxidation are assigned. Finally, we propose possible reaction mechanisms that could explain the formation of the intermediates and functional groups.

## 2. EXPERIMENTAL METHODS

The oxidation of [BMIM][DCBH] by nitrogen dioxide ( $\text{NO}_2$ ) was studied by exploiting an ultrasonic levitator apparatus at the University of Hawaii at Manoa. The levitator apparatus has been discussed in detail elsewhere.<sup>29,33,34</sup> Briefly, the apparatus utilizes a piezoelectric transducer oscillating at 58 kHz that generates a standing ultrasonic sound wave as a result of the waves reflecting between the transducer and a concave-shaped reflector.<sup>33</sup> The sound waves produce acoustic radiation pressure on the droplet, and the resulting acoustic force counteracts the gravitational force. Particles are therefore levitated slightly below the pressure nodes of the ultrasonic standing wave. The levitation device is enclosed in a process chamber, which allows levitation in various gases or gas mixtures of interest, including inert, highly reactive, or toxic gases.

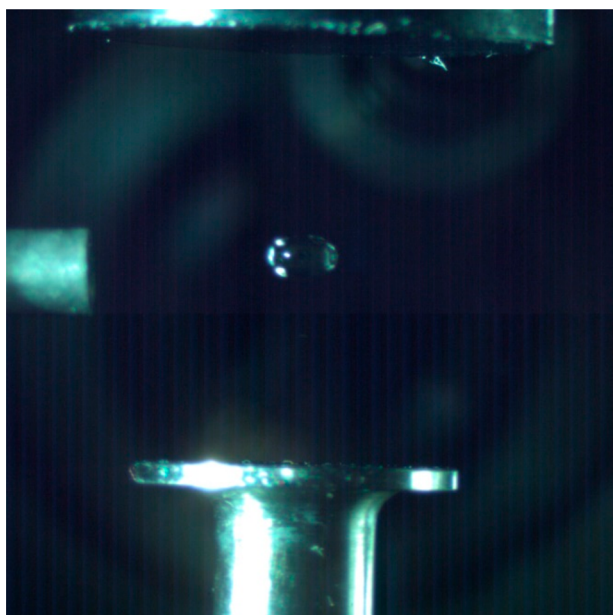


Figure 1. Photograph of a levitated droplet of [BMIM][DCBH].

The [BMIM][DCBH] ionic liquid was synthesized at Julius-Maximilian-Universität Würzburg (Germany) by a procedure similar to that used for the respective 1-ethyl-3-methylimidazolium salt.<sup>35</sup> Briefly, an equimolar solution containing 25.80 g (0.148 mol) of 1-butyl-3-methylimidazolium chloride ([BMIM]Cl) and 15.36 g (0.148 mol) of potassium dicyanodihydroborate<sup>36</sup> (K[DCBH]) dissolved in 150 mL of water was stirred at room temperature for 2 h. The ionic liquid was extracted from the reaction mixture with  $3 \times 50$  mL of dichloromethane ( $\text{CH}_2\text{Cl}_2$ ). The combined dichloromethane layers were dried with magnesium sulfate ( $\text{MgSO}_4$ ). Finally, the solvent was evaporated under reduced pressure, and the ionic liquid then dried under a vacuum ( $3 \times 10^{-3}$  mbar). The yield was 89%, and the purity was greater than 99.5% as determined by  $^1\text{H}$  and  $^{11}\text{B}$  NMR spectroscopy (Bruker DPX 400).

A [BMIM][DCBH] droplet was then levitated in a pressure minimum using a microliter droplet deposition system consisting of a syringe fixed to the process chamber and a needle attached to the end of a wobble stick.<sup>29</sup> In the present experiments, the droplet was levitated in either pure argon (Ar; Airgas, 99.9999%) or in a nitrogen dioxide and argon gas mixture consisting of 1.3%  $\text{NO}_2$  (Aldrich,  $\geq 99.5\%$ ) and 98.7%

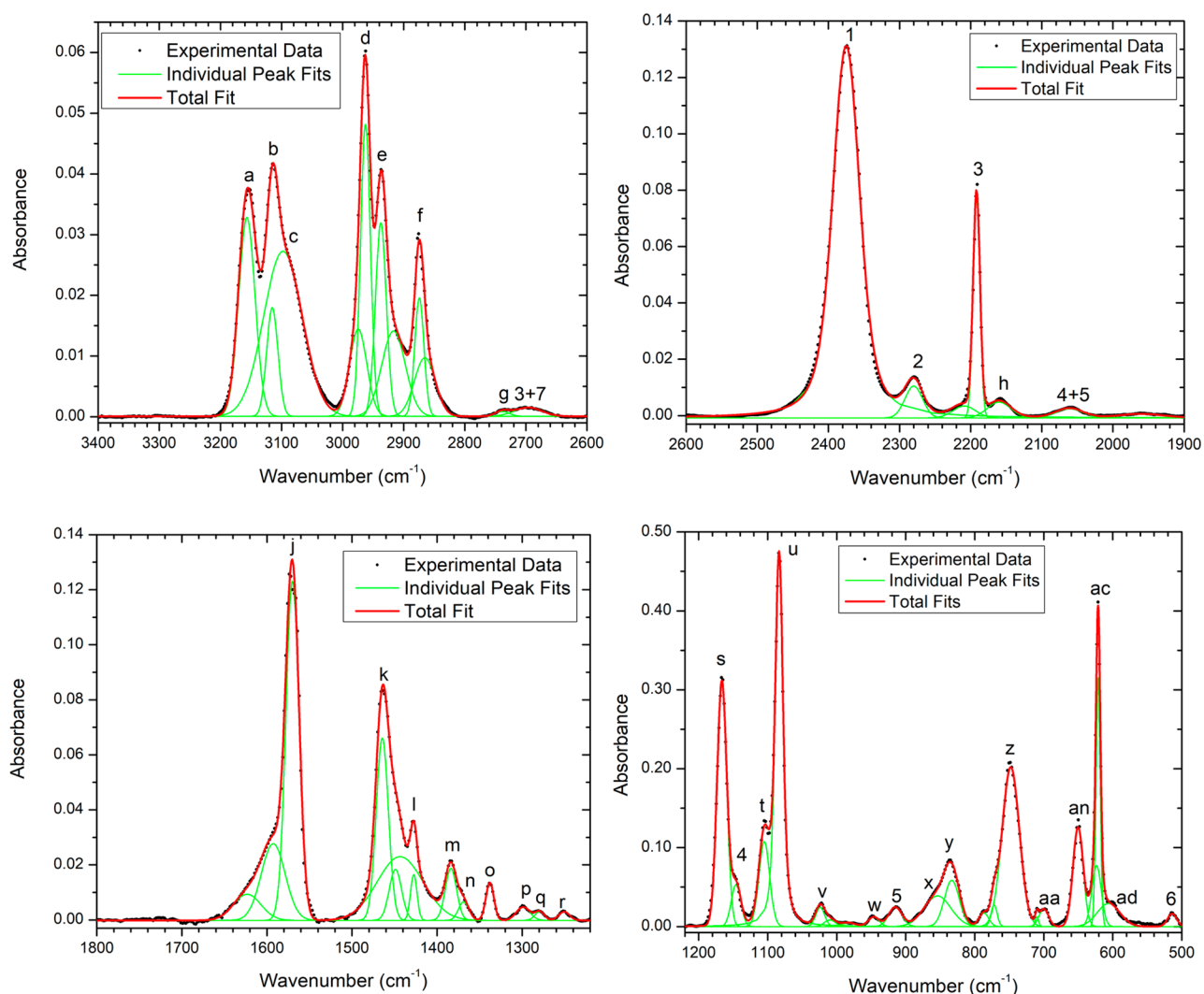


Figure 2. FTIR spectra of [BMIM][DCBH] together with the individual peak fits. The [BMIM]<sup>+</sup> peaks are labeled a–ad, and [DCBH]<sup>−</sup> peaks are labeled 1–6. The vibrational assignments are compiled in Table 1. The backgrounds were subtracted for clarity.

Ar at a total pressure of 880 Torr and temperature of 293 K. The levitated droplets were oblate spheroids with a mean horizontal diameter of  $3.2 \pm 0.4$  nm and mean vertical diameter of  $1.7 \pm 0.3$  nm (Figure 1).

The chemical effects of oxidizing [BMIM][DCBH] were studied with Raman, Fourier-transform infrared (FTIR), and UV-vis spectroscopies.<sup>29,37</sup> Raman spectra were collected using two different spectrometers operating at distinct excitation wavelengths. An *in situ* Raman spectrometer collected spectra of the levitated droplet using a Q-switched Nd:YAG laser emitting at a wavelength 532 nm. The Raman-shifted photons, backscattered from the droplet, were focused by a lens into a HoloSpec *f*/1.8 holographic imaging spectrograph equipped with a PI-Max 2 ICCD camera (Princeton Instruments). The spectra were collected simultaneously over the two wavenumber ranges from 300 to 2450  $\text{cm}^{-1}$  and 2400 to 4400  $\text{cm}^{-1}$  with a resolution of 9  $\text{cm}^{-1}$ .<sup>29</sup> The 532 nm laser beam can induce significant fluorescence in the samples, which might obscure the scattering peaks in the spectra. The Raman spectra of the ionic liquids were therefore also investigated *ex situ* using a micro-Raman RXN system (Kaiser Optical Systems), which operates at a wavelength of 785 nm and therefore produces significantly less fluorescence.<sup>37</sup> Each 785 nm Raman spectrum was collected in the 200–3500  $\text{cm}^{-1}$  Raman shift region for 10 s with 30 mW of laser power and a resolution of 8  $\text{cm}^{-1}$ . The FTIR spectra were collected in the wavenumber region of 400–4000  $\text{cm}^{-1}$  of a Nicolet 6700 FTIR spectrometer (Thermo Scientific).<sup>29</sup> *In situ* UV-vis reflectance spectra were recorded in the spectral region of 200–1100 nm using a StellarNet SILVER-Nova UV-vis monochromator, a Hamamatsu L10290 UV-vis fiber light source, and a Y-type fiber-optic reflectance probe.<sup>29</sup>

### 3. RESULTS AND DISCUSSION

**3.1. [BMIM][DCBH]. 3.1.1. Infrared Spectroscopy.** As a reference to interpret the spectra of the oxidized IL, it is first necessary to understand the spectrum of unreacted [BMIM][DCBH] (Figure 2). A fitting procedure was exploited to decompose the spectrum of unreacted [BMIM][DCBH] into its individual peaks. The best-fit wavenumbers of the absorption peaks are compiled in Table 1. Multiple regions exist in the spectra that contain numerous overlapping absorptions leading to degeneracy in the fitting procedure; therefore, only clearly defined peaks and prominent shoulders are reported. To our best knowledge, a detailed experimental study on the [BMIM][DCBH] ionic liquid has not been reported prior to this work. The [BMIM][DCBH] vibrational modes were therefore assigned by comparing the fitted peak wavenumbers with experimentally measured and theoretical values for structurally similar ionic liquids.<sup>29,38–42</sup> The fundamental modes of the [BMIM]<sup>+</sup> cation have been studied theoretically and experimentally both as an isolated ion and in different ionic pairs such as [BMIM][BF<sub>4</sub>] or [BMIM][PF<sub>6</sub>].<sup>29,38,42–46</sup> The assignments for the [BMIM]<sup>+</sup> cation in Tables 1 and 2 are based on ref 38 for [BMIM][BF<sub>4</sub>]. After accounting for small shifts in the peak positions produced by having a [BF<sub>4</sub>]<sup>−</sup> anion in place of a [DCBH]<sup>−</sup> anion, we found our [BMIM]<sup>+</sup> wavenumbers corresponded with sufficient accuracy to the values for [BMIM]<sup>+</sup> in [BMIM][BF<sub>4</sub>] as measured and calculated by Katsyuba *et al.* to permit assignments. In contrast to [BMIM]<sup>+</sup>, the vibrational modes of the [DCBH]<sup>−</sup> anion have not been extensively studied or completely assigned. The [DCBH]<sup>−</sup> anion was first synthesized by Spielvogel *et al.* incorporated into the salts sodium dicyanoborate (Na[DCBH]) and tetra-

**Table 1. Vibrational Mode Assignments for the Observed Peaks in the FTIR Spectra of [BMIM][DCBH]<sup>a</sup>**

peak label	present wavenumbers ( $\text{cm}^{-1}$ ) <sup>b</sup>	reference wavenumbers ( $\text{cm}^{-1}$ )	vibrational mode assignment <sup>c</sup>	ref
a	3157	3163	$\nu(\text{C4-H}), \nu(\text{C5-H})$ in-phase	38
b	3115	3123	$\nu(\text{C2-H})$	38
c	3098	3105	no assignment	38
d	2963	2966	$\nu_{\text{as}}(\text{CH}_2)$	38
e	2937	2942	$\nu_{\text{as}}(\text{CH}_2)$	38
f	2874	2878	$\nu_s[\text{CH}_3(\text{Bu})]$	38
g	$2738 \pm 4$	2738, 2736	combination mode, i.e., 2n, j + s	
3 + 7	$2696 \pm 4$	2705	combination mode, i.e., 3 + 7	
1	2375	2380	$\nu(\text{BH}), \text{B}_1$	39
2	2280	2260	$\nu(\text{BH}), \text{A}_1$	40
3	2192	2200	$\nu(\text{CN})$	39
h	$2161 \pm 6$	2168	combination mode, i.e., 2u	
4 + 5	$2061 \pm 3$	2061	combination mode, i.e., 4 + 5	
j	1570	1568	$\nu_{\text{as}}(\text{N1-C2-N3}), \tau(\text{C2-H})$	38
k	1464	1467	$\delta_s(\text{CH}_3)$	38
l	1427	1431	$\delta_s[\text{CH}_3(\text{Me})]$	38
m	1384	1387	$\omega(\text{CH}_2)$	38
n	$1369 \pm 3$	1373	$\nu(\text{C2-N1-CS})$	38
o	1338	1326	breathing, $\nu(\text{N-Bu}), \nu(\text{N-Me})$	38
p	$1299 \pm 2$	1300	$\tau(\text{CH}_2)$	38
q	$1279 \pm 3$	1270–1287	$r(\text{C-H}), t(\text{CH}_2)$	38
r	$1251 \pm 2$	1253	$\tau(\text{CH}_2), r(\text{C2-H})$	38
s	1166	1172	$\nu(\text{N-Bu}), \nu(\text{N-Me}), r(\text{C-H})$	38
4	1146	1145	$\delta(\text{BH})$	40
t	1105	1116	$r(\text{CH}_3), r[\text{CH}_3(\text{Bu})]$	38
u	1084	1093	$r(\text{CH})$	38
v	$1023 \pm 9$	1022–1036	$\delta(\text{ring})$	38
w	946	948	$r[\text{CH}_3(\text{Bu})], r(\text{CH}_2)$	38
5	915	937	$\nu_{\text{as}}(\text{BC})$	41
x	$854 \pm 6$	849	$\gamma(\text{C4-H}), \gamma(\text{C5-H})$	38
y	833	835	$\nu_s(\text{C-C-C})$	38
z	748	755	$r(\text{CH}_2)$	38
aa	700	697	$\nu(\text{N-Me}), \nu(\text{N-Bu})$	38
ab	650	651	$\gamma(\text{N-Me}), \gamma(\text{N-Bu})$	38
ac	621	623	$\gamma(\text{N-Bu}), \text{ring-puckering}$	38
ad	$605 \pm 6$	600	$\delta(\text{N1-C2-N3})$	38
6	514	496	$\delta(\text{BCN})$	42

<sup>a</sup>The assignments are based on refs 38–42. <sup>b</sup>The uncertainties are equal to, or less than, 1  $\text{cm}^{-1}$  unless stated otherwise. <sup>c</sup>Key:  $\nu$ , stretching;  $\delta$ , bending;  $r$ , rocking;  $\omega$ , wagging;  $\tau$ , torsion;  $s$ , symmetric;  $as$ , antisymmetric.

butylammonium dicyanoborate ([*n*-Bu<sub>4</sub>N][DCBH]).<sup>39</sup> These authors did not conduct a detailed characterization of the infrared spectra of the [DCBH]<sup>−</sup> salts but identified only the B–H and C–N stretching modes at 2380 and 2200  $\text{cm}^{-1}$ , respectively. However, Berschied *et al.* used Raman and IR spectroscopies to study in more detail the vibrational modes of

Table 2. Vibrational Mode Assignments for the Observed Peaks in the Raman Spectra of [BMIM][DCBH] at the Excitation Wavelengths of 532 and 785 nm<sup>a</sup>

peak label	present wavenumbers (cm <sup>-1</sup> ) <sup>b</sup>		reference wavenumbers (cm <sup>-1</sup> )	vibrational mode assignment <sup>c</sup>	ref
	excitation wavelength				
	785 nm	532 nm			
a	3170	3170	3173	$\nu(\text{C4-H}), \nu(\text{C5-H})$ in-phase	38
b	3115	3114	3127	$\nu(\text{C2-H})$	38
c	2963	2962	2969	$\nu_{\text{as}}(\text{CH}_2)$	38
d	2941	2939	2942	$\nu_{\text{as}}(\text{CH}_2)$	38
e	2914	2917	2917	$\nu_s[\text{CH}_3(\text{Me})]$	38
f	2874	2875	2877	$\nu_s[\text{CH}_3(\text{Bu})]$	38
g	2837	2836	2840	$\nu_s(\text{CH}_2)$	38
h	2741	2741	2731	combination mode, i.e., i + t	
1	2378	2375	2380	$\nu(\text{BH}), \text{B}_1$	39
2	2278	2284	2258	$\nu(\text{BH}), \text{A}_2$	40
3	2194	2194	2200	$\nu(\text{CN})$	39
i	2153	2158	2169	combination mode, i.e., v + z	
j	1568	1573	1568	$\nu_{\text{as}}(\text{N1-C2-N3}), \text{r}(\text{C2-H})$	38
k	1458	1453	1448	$\delta_s[\text{CH}_3(\text{Me})]$	38
l	1443	1449	1439–1447	$\delta_s(\text{CH}_2)$	38
m	1418	1421	1421	$\nu(\text{ring}), \delta[\text{CH}_2]$	38
n	1389	1392	1391	$\omega(\text{CH}_2)$	38
o	1338	1340	1342	breathing, $\nu(\text{N-Bu}), \nu(\text{N-Me})$	38
p	1312 ± 2	1311	1311	$\omega(\text{CH}_2)$	38
q	1302 ± 2	–	1303	$\tau(\text{CH}_2)$	38
r	1281	1281	1286	$\text{r}(\text{C-H}), \text{t}(\text{CH}_2)$	38
s	1252	1252	1254	$\tau(\text{CH}_2), \text{r}(\text{C2-H})$	38
t	1210	1210	1212	$\tau(\text{CH}_2)$	38
u	1163	1166	1173	$\nu(\text{N-Bu}), \nu(\text{N-Me}), \text{r}(\text{C-H})$	38
v	1146	1146	1148	$\text{r}(\text{CH}_3)$	38
w	1115	1114	1117	$\text{r}(\text{CH}_3), \text{r}[\text{CH}_3(\text{Bu})]$	38
x	1089	1088	1093	$\text{r}(\text{C-H})$	38
			1088	$\delta(\text{CH}), \nu_{\text{as}}(\text{ring})$	
y	1056	1055	1057	$\nu(\text{C-C})$	38
z	1023	1023	1011	breathing, $\nu(\text{N-Bu}), \nu(\text{N-Me})$	38
aa	980	980	976	$\nu_{\text{as}}(\text{C-C})$	38
ab	946	944 ± 2	951	$\text{r}[\text{CH}_3(\text{Bu})], \text{r}(\text{CH}_2)$	38
4	907	905	937	$\nu_{\text{as}}(\text{BC})$	41
ac	884	882 ± 2	884	$\nu(\text{C-C})$	38
ad	858 ± 3	856 ± 20	849	$\gamma(\text{C4-H}), \gamma(\text{C5-H})$	38
ae	825	824	825	$\nu_2(\text{C-C-C})$	38
af	809	807	810	$\nu_2(\text{C-C-C})$	38
ag	791	790	810	$\nu_3(\text{C-C-C})$	38
ah	752	752	741–760	$\text{r}(\text{CH}_2)$	38
ai	736	739 ± 2	734	$\text{r}(\text{CH}_2)$	38
aj	698	700	699	$\nu(\text{N-Me}), \nu(\text{N-Bu})$	38
ak	658	656	658	$\nu(\text{N-Me}), \nu(\text{N-Bu})$	38
al	623	622	624	$\gamma(\text{N-Bu}), \text{ring puckering}$	38
am	600	600	601	$\delta(\text{N1-C2-N3})$	38
5	515	512	521	$\delta(\text{BCN})$	41
an	501 ± 2	–	501	$\delta(\text{N-C-C}), \delta(\text{C-C-C})$	38
ao	477	–	473	$\delta(\text{N-C-C}), \delta(\text{C-C-C})$	38
ap	434	429 ± 5	435	$\text{r}(\text{N-Bu}), \text{r}(\text{N-Me}), \delta(\text{N-C-C}), \delta(\text{C-C-C})$	38
aq	413	413 ± 2	415	$\text{r}(\text{N-Bu}), \text{r}(\text{N-Me})$	38
6	351	352	358	$\delta(\text{BCN})$	40
ar	325	327	325	$\delta(\text{C-C-C})$	38
as	280	287	282	$\tau(\text{Bu})$	38
at	256	256	257	$\gamma(\text{N-Me}), \delta(\text{C-C-C})$	38

<sup>a</sup>The assignments are based on refs 38–41. <sup>b</sup>The uncertainties are equal to, or less than, 1 cm<sup>-1</sup> unless stated otherwise. <sup>c</sup>Key:  $\nu$ , stretching;  $\delta$ , bending;  $\text{r}$ , rocking;  $\omega$ , wagging;  $\tau$ , torsion;  $\text{s}$ , symmetric;  $\text{as}$ , antisymmetric.

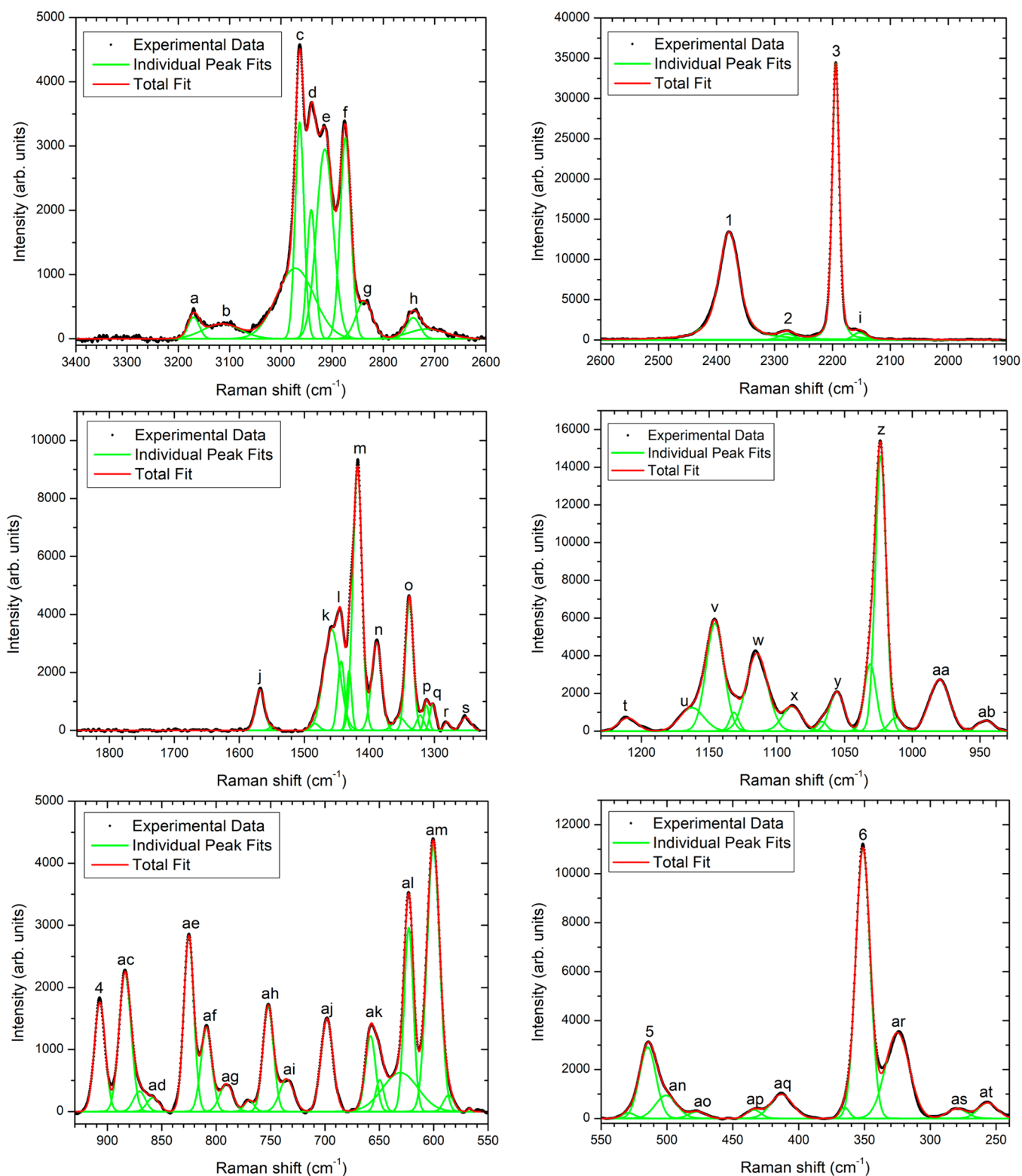


**Figure 3.** Raman spectra of [BMIM][DCBH] excited by a wavelength of 785 nm. The individual peak fits are included. The [BMIM]<sup>+</sup> peaks are labeled a–at, and the [DCBH]<sup>−</sup> peaks are labeled 1–6. The vibrational assignments are compiled in Table 2.

[BH<sub>3</sub>CN]<sup>−</sup>.<sup>40</sup> The tetracyanoborate anion ([B(CN)<sub>4</sub>]<sup>−</sup>) represents the most studied anion that is structurally similar to [DCBH]<sup>−</sup>.<sup>41,47–52</sup> The ions [BH<sub>3</sub>CN]<sup>−</sup> and [B(CN)<sub>4</sub>]<sup>−</sup> have bonds similar to [DCBH]<sup>−</sup>; that is, [BH<sub>3</sub>CN]<sup>−</sup> includes both B–H and B–CN bonds, whereas [B(CN)<sub>4</sub>]<sup>−</sup> contains only B–CN bonds. These previous studies of the anions [BH<sub>3</sub>CN]<sup>−</sup> and

[B(CN)<sub>4</sub>]<sup>−</sup> were therefore used to assign the FTIR spectra of [DCBH]<sup>−</sup> (Figure 2 and Table 1).

The high-wavenumber region of the spectra from 2800 to 3200 cm<sup>−1</sup> corresponds to the C–H stretching modes of the [BMIM]<sup>+</sup> cation.<sup>29,38</sup> The region from 3000 to 3200 cm<sup>−1</sup> is produced by the C–H stretching modes associated with the

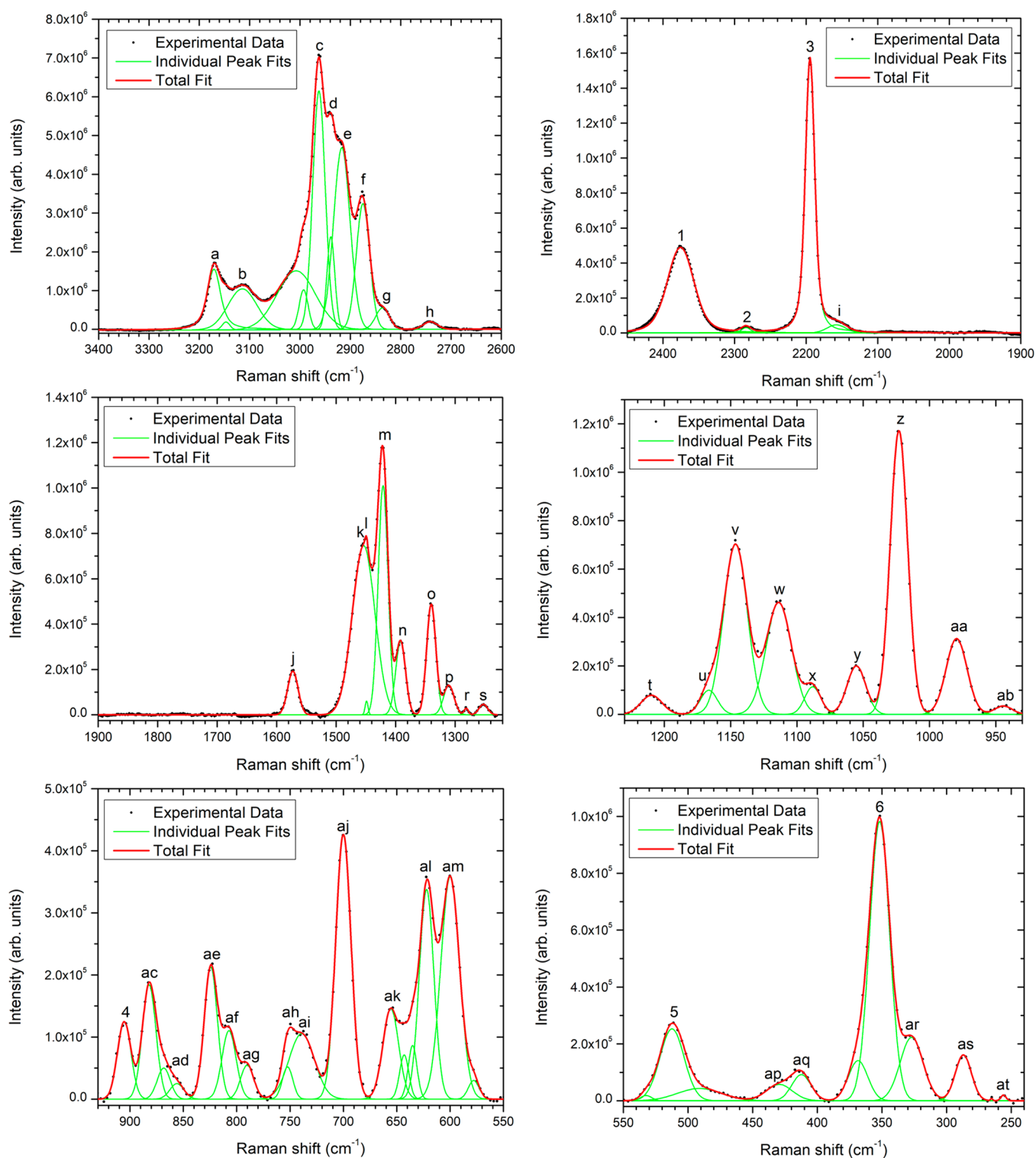


**Figure 4.** Raman spectra of a [BMIM][DCBH] droplet levitated in argon excited by a wavelength of 532 nm. The individual peak fits are included. The [BMIM]<sup>+</sup> peaks are labeled a–at, and [DCBH]<sup>−</sup> peaks are labeled 1–6. The vibrational assignments are compiled in Table 2. The backgrounds were subtracted for clarity.

imidazolium ring, whereas the region from 2800 to 3000 cm<sup>−1</sup> results from the C–H stretching modes of the butyl and methyl side chains. The spectral region of the imidazolium ring contains two prominent peaks at 3157 and 3115 cm<sup>−1</sup>, which can be assigned to the C(4),(5)–H and C(2)–H stretching modes, respectively. The spectral region corresponding to fundamentals of the side chains exhibits three peaks at 2963, 2937, and 2874

cm<sup>−1</sup>, which can be assigned to C–H stretching modes of the CH<sub>2</sub> and CH<sub>3</sub> groups of the butyl chain. Although the asymmetric C–H stretching of the methyl group is expected at 3015 cm<sup>−1</sup>, no clear absorption is revealed in Figure 2.<sup>29</sup> The vibrational modes associated with the imidazolium ring of the [BMIM]<sup>+</sup> cation are pronounced in the 600–1600 cm<sup>−1</sup> region; for example, the ring modes are labeled ai, w, s, and n at 621,

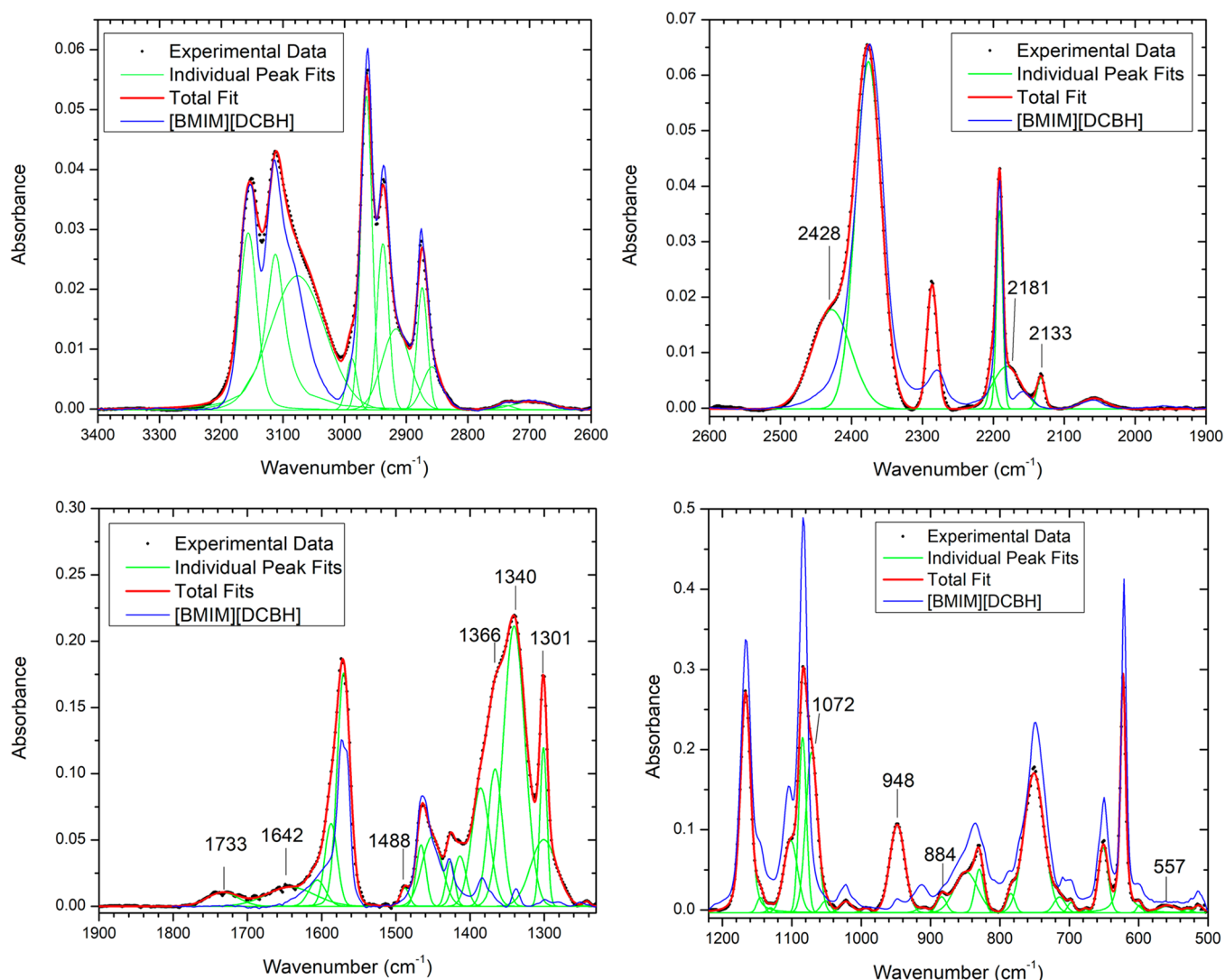


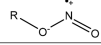
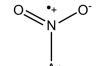
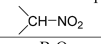
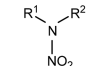
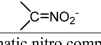
**Figure 5.** FTIR spectra of [BMIM][DCBH] and individual peak fits after reaction with nitrogen dioxide. The spectra of unreacted [BMIM][DCBH] (blue lines) are shown for comparison. The wavenumbers of the newly formed peaks are identified, and the vibrational assignments are shown in Table 3. The backgrounds were subtracted for clarity. The unreacted spectrum in the 2600–1900  $\text{cm}^{-1}$  region is scaled by a factor of 0.5.

1167, 1338, and 1570  $\text{cm}^{-1}$ , respectively. The main [DCBH]<sup>−</sup> anion vibrational peaks occur in the spectral region from 2150 to 2400  $\text{cm}^{-1}$ .<sup>39,40</sup> The two most intense [DCBH]<sup>−</sup> peaks are 3 at 2192  $\text{cm}^{-1}$  and 1 at 2375  $\text{cm}^{-1}$ , which are assigned to C–N and B–H stretching modes, respectively.<sup>39–41</sup> Additionally, there are two smaller peaks on the lower-wavenumber sides of the C–N and B–H fundamentals, which are labeled 4 and 2 and centered at 2161 and 2280  $\text{cm}^{-1}$ , respectively. The separation of peaks 1 and 2 at 95  $\text{cm}^{-1}$  is larger than the isotopic shift of 20  $\text{cm}^{-1}$  that occurs between the <sup>10</sup>B–H and <sup>11</sup>B–H stretching modes; therefore, peak 2 cannot be assigned to the <sup>11</sup>B–H stretching mode.<sup>40</sup> However, the two B–H stretching modes, E and A<sub>1</sub>, in the [BH<sub>3</sub>CN]<sup>−</sup> ion with the point group of C<sub>3v</sub> are separated by 90  $\text{cm}^{-1}$ .<sup>40</sup> Similarly, peaks 1 and 2 might be produced by B–H stretching modes with different symmetries, for example B<sub>1</sub> and A<sub>1</sub>, in the [DCBH]<sup>−</sup> anion of point group C<sub>2v</sub> (Table 1). In contrast, peak h at 2161  $\text{cm}^{-1}$  appears to be a combination band of 2u. The peak labeled “4 + 5” at 2061  $\text{cm}^{-1}$  occurs in the region where a  $\nu(\text{NC})$  vibrational mode produced by an isocyano attachment to boron (B–NC) is expected at 2065  $\text{cm}^{-1}$ ,<sup>39</sup> but there are no signs of an isocyano group in the

NMR spectra used to determine the purity of the [BMIM]-[DCBH] sample (Supporting Information); also, this feature does not appear in the Raman spectra of [BMIM][DCBH] (Figures 3 and 4). The absence of an isocyano vibrational mode is consistent with the characterization of the [DCBH]<sup>−</sup> salts synthesized by Spielvogel *et al.*<sup>39</sup> Therefore, the peak labeled “4 + 5” is likely a combination band of peaks 4 and 5. The [DCBH]<sup>−</sup> anion also produced peaks at 513 and 1147  $\text{cm}^{-1}$ , which are assigned to the BCN bending mode and B–H bending mode, respectively.

**3.1.2. Raman Spectroscopy.** Raman spectra of [BMIM]-[DCBH] were recorded at the excitation wavelengths of 532 and 785 nm, and the resulting spectra are shown in Figures 3 and 4, respectively. The peak positions obtained by fitting to the spectra are compiled in Table 2. Following a procedure similar to that in section 3.1.1 for the FTIR spectra, the vibrational modes are assigned in Table 2 for the [BMIM]<sup>+</sup> cation by comparison with ref 38 and for the [DCBH]<sup>−</sup> anion using the measurements of refs 39–41. The peak wavenumbers for the excitation wavelengths of 532 and 785 nm are almost identical, and therefore, for clarity, in this section the wavenumbers will be

**Table 3.** Assignments of the New Vibrational Modes in the FTIR Spectra of [BMIM][DCBH] after Reaction with 1.3% NO<sub>2</sub><sup>a</sup>

Experimental Wavenumber (cm <sup>-1</sup> ) <sup>b</sup>	Functional Group / Molecule	Region (cm <sup>-1</sup> )	Vibrational Modes <sup>c</sup>	Ref.
2428	BH or BH <sub>2</sub>	2630–2350	$\nu(\text{B-H})$	59
2181	NCO <sup>-</sup>	2225–2100	$\nu_{\text{as}}(\text{NCO})$	53
2133	NCO <sup>-</sup>	2225–2100	$\nu_{\text{as}}(\text{NCO})$	53
1733	N <sub>2</sub> O <sub>4</sub>	1735	$\nu_9$	55
1642 ± 9	Organic nitrites 	1680–1610	$\nu(\text{N=O})$	60
1488 ± 3	Aromatic nitro compounds 	1555–1487	$\nu_{\text{as}}(\text{NO}_2)$	60
1488 ± 3	Covalent B–N compounds	1550–1330	$\nu(\text{B-N})$	53
1366 ± 9	Covalent B–N compounds	1550–1330	$\nu(\text{B-N})$	53
1366 ± 9	Aliphatic nitro compounds 	1381–1310	$\nu_{\text{s}}(\text{NO}_2)$	53, 60
1366 ± 9	B–O	1380–1310	$\nu(\text{B-O})$	53
1340	Covalent B–N compounds	1550–1330	$\nu(\text{B-N})$	53, 59
1340	B–O	1380–1310	$\nu(\text{B-O})$	53
1340	Aliphatic nitro compounds	1381–1310	$\nu_{\text{s}}(\text{NO}_2)$	53, 60
1340	Aromatic nitro compounds	1357–1318	$\nu_{\text{s}}(\text{NO}_2)$	53
1301	Nitroamines 	1315–1260	$\nu_{\text{s}}(\text{NO}_2)$	53
1072	Aromatic nitro compounds	1180–865	$\nu(\text{CN})$	53
1072	Carbonitrates 	1175–1040	$\nu_{\text{s}}(\text{NO}_2)$	53
948	Aromatic nitro compounds	1180–865	$\nu(\text{CN})$	53
948	Aliphatic nitro compounds	1000–915	$\nu(\text{CN})$	53
884	Organic nitro compounds	890–835	NO <sub>2</sub> scissor	61
557 ± 2	Aliphatic nitro compound	560–470	Out-of-plane wag	53, 60

<sup>a</sup>The functional groups, regions of maximum absorption, and vibrational modes are obtained from Refs 51, 53, 60, 61. <sup>b</sup>The uncertainties are equal to, or less than, 1 cm<sup>-1</sup> unless stated otherwise. <sup>c</sup>Key:  $\nu$ , stretching;  $\nu_{\text{s}}$ , symmetric;  $\nu_{\text{as}}$ , antisymmetric.

reported only for the 532 nm spectra. The Raman spectra can be separated into three spectral regions: 250–1600 cm<sup>-1</sup>, 2100–2400 cm<sup>-1</sup>, and 2700–3200 cm<sup>-1</sup>. The Raman spectra in the higher-wavenumber region from 2700 to 3200 cm<sup>-1</sup> have similar features as the FTIR spectra in the same spectral region. However, in contrast to the FTIR spectra, the relative intensities produced by the C–H stretching modes of the imidazolium ring from 3000 to 3200 cm<sup>-1</sup> are significantly weaker compared to the C–H stretching modes of the butyl and methyl side chains between 2800 and 3000 cm<sup>-1</sup>. Furthermore, the symmetric C–H stretching of the methyl group is prominent in the Raman spectrum at 2917 cm<sup>-1</sup>, but the same mode is not evident in the FTIR spectrum. In the 2100–2400 cm<sup>-1</sup> region characteristic of the [DCBH]<sup>-</sup> fundamentals, there is one main difference between the FTIR and Raman spectra; that is, the C–N stretching mode at 2194 cm<sup>-1</sup> in the Raman spectra is much larger than the B–H stretching mode at 2375 cm<sup>-1</sup>, whereas the reverse is true in the FTIR spectra with the B–H stretching mode dominant. The [DCBH]<sup>-</sup> features present in both the Raman and FTIR spectra include the asymmetric B–C stretching mode at 905 cm<sup>-1</sup> and the BCN bending modes at 512 and 352 cm<sup>-1</sup>.<sup>40,41</sup> The lower-wavelength region from 250 to 1600 cm<sup>-1</sup> reveals mainly vibrational modes of the imidazolium ring, which are stronger in the Raman spectra than in the FTIR spectra, for example, the  $\nu(\text{ring}) + \delta(\text{CH}_2)$ , breathing +  $\nu(\text{N-Bu}) + \nu(\text{N-Me})$ , and breathing +  $\nu(\text{N-Bu}) + \nu(\text{N-Me})$  vibrational modes at 1421, 1340, and 1023 cm<sup>-1</sup>, respectively.

**3.2. [BMIM][DCBH] Oxidation.** **3.2.1. Infrared Spectroscopy.** A droplet of [BMIM][DCBH] was levitated in a gas mixture containing 1.3% NO<sub>2</sub> and 98.7% argon and allowed to react. The FTIR spectra of the oxidized [BMIM][DCBH] sample are shown in Figure 5 together with the individual peak fits. The unreacted [BMIM][DCBH] spectra (blue lines) are included in Figure 5 for comparison. Comparing the spectra before and after the reaction reveals that numerous new peaks were produced by the oxidation. The best-fit wavenumbers of the new peaks are identified in Figure 5 and compiled in Table 3. Owing to the complexity of the spectra for the oxidized ionic liquid, it is unlikely that IR or Raman spectroscopy alone can identify the individual product molecules, but the techniques can help to determine which *functional groups* formed during the oxidation process. The simplest reaction mechanism to form the products would involve a nitrogen or oxygen atom of NO<sub>2</sub> bonding to a carbon, nitrogen, or boron atom of [BMIM]-[DCBH]. The possible functional groups required to account for the new peaks would then be limited to the organic nitro-compounds and the B–N and B–O containing compounds. The vibrational modes of the functional groups of the organic nitro-compounds and the B–N and B–O containing compounds with wavenumber regions including the new peaks are compiled in Table 3.

The most intense new absorption feature occurs in the region of 1260–1400 cm<sup>-1</sup> (Figure 5) and contains a sharp peak at 1301 cm<sup>-1</sup> and a broader peak at 1340 cm<sup>-1</sup> with a shoulder at 1366 cm<sup>-1</sup>. The symmetric NO<sub>2</sub> stretching mode of the nitroamines could account for the peak at 1301 cm<sup>-1</sup>. The broader feature at 1340 cm<sup>-1</sup> with a shoulder at 1366 cm<sup>-1</sup> could be produced by the symmetric NO<sub>2</sub> stretching modes of the organic nitro-compounds including the dinitroalkanes (1375–1325 cm<sup>-1</sup>), aliphatic (RNO<sub>2</sub>; 1381–1310 cm<sup>-1</sup>) compounds, and aromatic (ArNO<sub>2</sub>; 1357–1318 cm<sup>-1</sup>) compounds, and also the B–N stretching of B–N containing compounds (1550–1330 cm<sup>-1</sup>) or the B–O stretching of B–O containing compounds (1380–1310 cm<sup>-1</sup>).<sup>53</sup>

Another significant change in the FTIR spectra caused by the oxidation occurs in the 1900–2600 cm<sup>-1</sup> region associated with the fundamental modes of the [DCBH]<sup>-</sup> anion. The peak heights corresponding to the B–H and C–N stretching modes at 2375 and 2192 cm<sup>-1</sup>, respectively, decreased by a factor of 2 following oxidation, suggesting that the [DCBH]<sup>-</sup> anion was partially degraded by reaction with NO<sub>2</sub>. Note that the unreacted spectrum of the ionic liquid in this region was scaled by a factor of 0.5 in Figure 5. In addition to the decrease in intensity, two new absorption features formed at 2133 and 2428 cm<sup>-1</sup>. The peak at 2428 cm<sup>-1</sup> occurs where BH and BH<sub>2</sub> stretching modes are predicted, while the peak 2133 cm<sup>-1</sup> appears in the region of asymmetric CNO stretching of NCO<sup>-</sup>.<sup>53</sup> The new peak in the B–H stretching region provides further evidence that the reaction involves the boron-containing anion, [DCBH]<sup>-</sup>. In contrast, the C–H stretching region of the [BMIM]<sup>+</sup> cation in the range of 2600–3400 cm<sup>-1</sup> shows no significant change in intensity; therefore, the [BMIM]<sup>+</sup> cation reacted to a lesser extent than the [DCBH]<sup>-</sup> anion.

The broad, unresolved new peak at 1733 cm<sup>-1</sup> is outside the range of the organic nitro-compounds.<sup>53</sup> The 1700–1800 cm<sup>-1</sup> wavenumber range represents, however, an active region for the stretching modes of the carbonyl functional group (C=O).<sup>53</sup> The new peak at 1733 cm<sup>-1</sup> could therefore be assigned to C=O functional groups formed by higher-order reactions and oxidation. Alternatively, the new structure in the 1700–1800

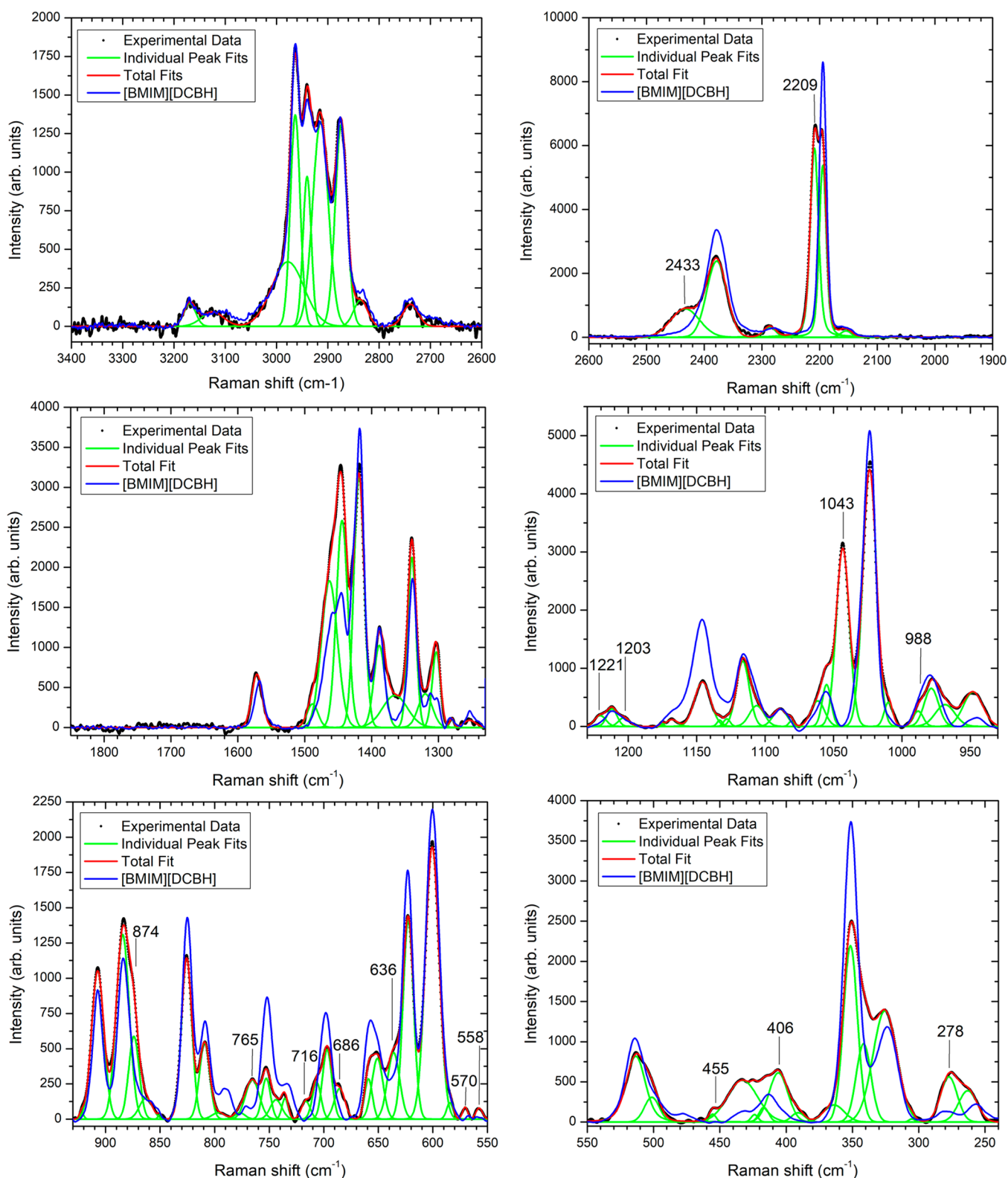


**Figure 6.** Raman spectra at the 785 nm excitation wavelength of [BMIM][DCBH] after reaction with nitrogen dioxide. The individual peak fits are included. The spectra of the unreacted [BMIM][DCBH] (blue lines) are shown for comparison. The wavenumbers of the newly formed peaks are identified, and the vibrational assignments are shown in Table 4. All the unreacted spectra were scaled for clarity.

$\text{cm}^{-1}$  region could be caused by dinitrogen tetroxide ( $\text{N}_2\text{O}_4$ ) dissolved in the droplet.<sup>28,29,54</sup> More specifically, the  $\nu_5$  and  $\nu_9$  vibrational modes of  $\text{N}_2\text{O}_4$  occur at 1718 and 1735  $\text{cm}^{-1}$  and thus could account for the peak at 1733  $\text{cm}^{-1}$ .<sup>55</sup> Our previous studies on the [DCA]<sup>-</sup>-based ionic liquids revealed multiple

resolved peaks in the 1700–1800  $\text{cm}^{-1}$  wavenumber region that were assigned to the C=O functional group or  $\text{N}_2\text{O}_4$  vibrational modes; therefore, the unresolved structure here is likely a combination of the same modes.<sup>28,29,54</sup>

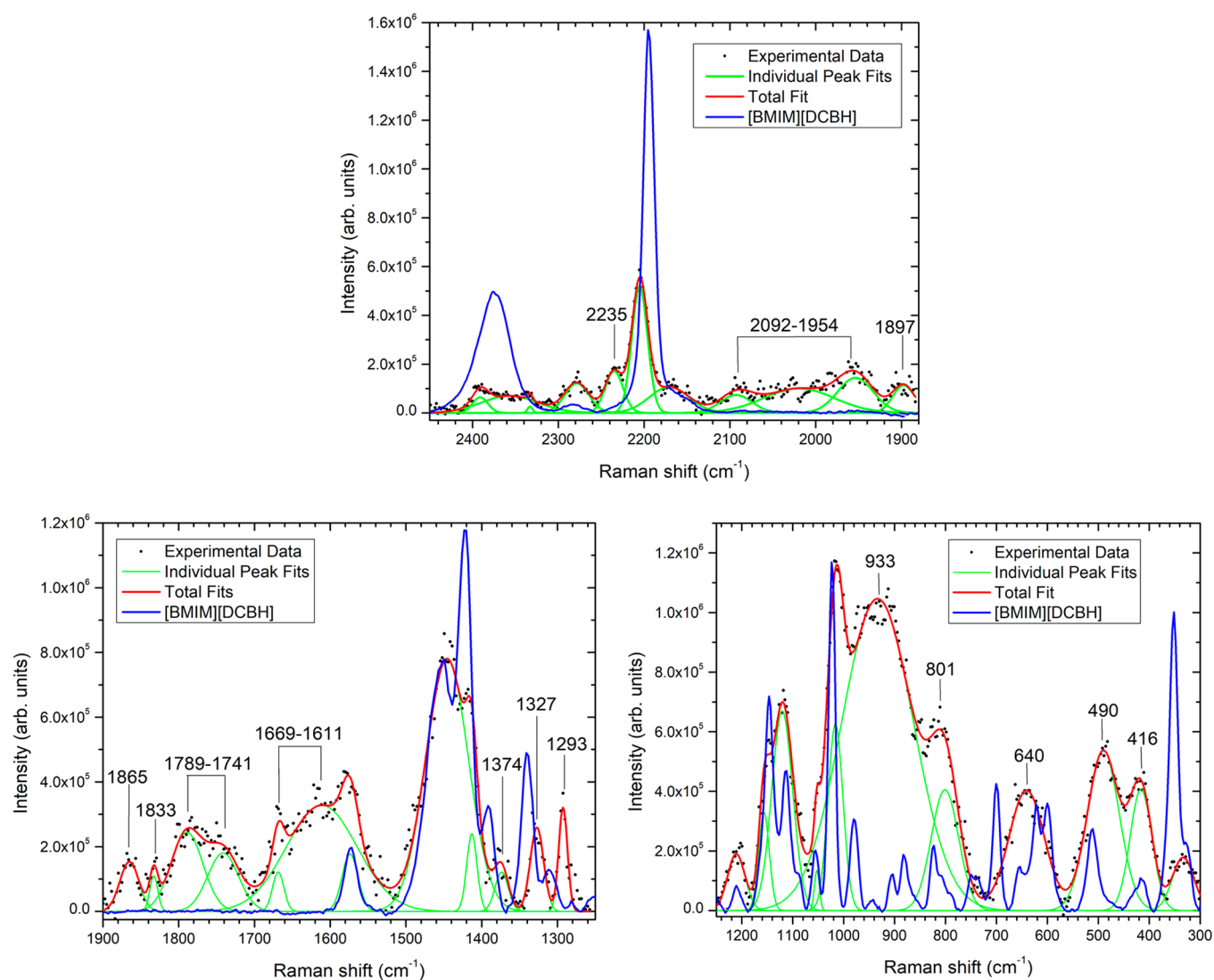


**Figure 7.** Raman spectra at the 532 nm excitation wavelength of [BMIM][DCBH] after reaction with nitrogen dioxide. The individual peak fits are included. The spectra of the unreacted [BMIM][DCBH] (blue lines) are shown for comparison. The wavenumbers of the newly formed peaks are identified, and the vibrational assignments are presented in Table 4. The backgrounds were removed for clarity.

**3.2.2. Raman Spectroscopy.** Raman spectra recorded at excitation wavelengths of 785 and 532 nm for the [BMIM][DCBH] droplet after oxidation by nitrogen dioxide are shown in Figures 6 and 7, respectively, together with the individual peak fits and the unreacted [BMIM][DCBH] spectra (blue lines). The wavenumbers of the new peaks and suggested peak assignments for the 785 and 532 nm spectra are compiled in Tables 4 and 5, respectively. The vibrational modes of the new peaks were assigned using essentially the same procedure as discussed in section 3.2.1 for the FTIR spectra. As for the FTIR data, most of the new peaks are likely caused by the organic nitro-compounds, B–N compounds, and B–O compounds. The possible newly formed nitro-compounds include the aromatic nitro compounds ( $\text{ArNO}_2$ ), aliphatic nitro compounds ( $\text{RNO}_2$ ), nitroamines ( $\text{R}^1\text{R}^2\text{NNO}_2$ ), organic nitrites ( $\text{RONO}$ ), and carbonitrates ( $\text{R}^1\text{R}^2\text{C}=\text{NO}_2^-$ ). The functional groups of the organic nitro-compounds produce features only in the 1700–475  $\text{cm}^{-1}$  spectral region,<sup>53</sup> while the B–H stretching modes are Raman active only in the ranges of 2350–2630  $\text{cm}^{-1}$ . To assign the 2350–1700  $\text{cm}^{-1}$  and 475–300  $\text{cm}^{-1}$  spectral regions, moieties were therefore chosen that formed part of the organic

nitro-compounds or boron-containing compounds likely to be produced by reaction between [BMIM][DCBH] and nitrogen dioxide (Table 5). Finally, unreacted [BMIM][DCBH] might contribute to the final spectrum after oxidation in wavenumber regions where the original molecule produced large peaks.

**3.2.3. Ultraviolet–Visible Spectroscopy.** In addition to vibrational spectroscopy studied by FTIR and Raman methods, we used *in situ* UV–vis reflectance spectroscopy to provide information about changes in the electronic structure induced by oxidation of [BMIM][DCBH] with nitrogen dioxide. The UV–vis reflectance spectra before (black line) and after (red line) the reaction were recorded in the wavelength region of 200–1100 nm and are shown in Figure 8a. The spectrum of unreacted [BMIM][DCBH] in Figure 8a (black line) has a minimum in the reflectance (corresponding to a maximum in the absorption) in the spectral range of approximately 220–310 nm. Bernhardt *et al.* recorded the UV–vis spectra of potassium tetracyanoborate ( $\text{K}[\text{B}(\text{CN})_4]$ ) and tetrabutylammonium ( $[\text{Bu}_4\text{N}][\text{B}(\text{CN})_4]$ ) salts, which have structures relevant to [DCBH].<sup>51</sup> The only absorption feature for both salts occurs in the UV spectral region of 190–240 nm and was assigned to  $n_{\text{N}}$

**Table 4. Assignments of the New Peaks in the 785 nm Raman Spectrum of [BMIM][DCBH] Produced by Reaction with 1.3% NO<sub>2</sub> and 98.7% Argon<sup>a</sup>**

present wavenumbers (cm <sup>-1</sup> ) <sup>b</sup>	functional group/molecule	region (cm <sup>-1</sup> )	vibrational modes <sup>c</sup>	ref
2433	BH & BH <sub>2</sub>	2630–2350	$\nu$	59
2209	NCO <sup>-</sup>	2225–2100	$\nu_{\text{as}}(\text{NCO})$	53
2209	unreacted [BMIM][DCBH]	2194	see Table 2	
1488 ± 2	aromatic nitro compounds	1580–1485	$\nu_{\text{as}}(\text{NO}_2)$	53
1488 ± 2	covalent B–N compounds	1550–1330	$\nu(\text{BN})$	53
1221 ± 3	carbonitrates	1315–1205	$\nu_{\text{as}}(\text{NO}_2)$	53
1203 ± 2	carbonitrates	1315–1205	$\nu_{\text{as}}(\text{NO}_2)$	53
1043	aromatic nitro compounds	1180–865	$\nu(\text{CN})$	53
1043	carbonitrates	1175–1040	$\nu_{\text{s}}(\text{NO}_2)$	53
988	aromatic nitro compounds	1180–865	$\nu(\text{CN})$	53
988	aliphatic nitro compounds	1000–915	$\nu(\text{CN})$	53
988	nitroamines	1030–980	$\nu(\text{N–N})$	53
988	boronic acids	~1000	$\nu(\text{B–OH})$	53
874 ± 2	aromatic nitro compounds	1180–865	$\nu(\text{CN})$	53
874 ± 2	aliphatic nitro compounds	920–850	$\nu(\text{CN})$	53
765 ± 3	B–OH, boronic acids	800–700		53
765 ± 3	nitroamines	775–755	NO <sub>2</sub> def.	53
716 ± 3	B–OH, boronic acids	800–700		53
716 ± 3	nitroamines	730–590	$\omega(\text{NO}_2)$	53
716 ± 3	carbonitrates	735–700	NO <sub>2</sub> def.	53
686	nitroamines	730–590	$\omega(\text{NO}_2)$	53
636	nitroamines	730–590	$\omega(\text{NO}_2)$	53
636	aliphatic nitro compounds	655–605	NO <sub>2</sub> def.	53
570	nitroamines	620–560	$r(\text{NO}_2)$	53
570	aromatic nitro compounds	590–500	in-plane $\delta(\text{NO}_2)$	53
558	aromatic nitro compounds	590–500	in-plane $\delta(\text{NO}_2)$	53
558	aliphatic nitro compounds	560–470	$r(\text{NO}_2)$	53
455	O=N–N=C	455	$\nu_4 + \nu_5 + \nu_6$	62
406	N <sub>2</sub> O <sub>4</sub>	425	$\nu_7$	63
278	N <sub>2</sub> O <sub>4</sub>	270	$\nu_{10}$	63
278	O=N–C≡N	264	torsion, $\nu_7$	64
278	O=N–N=C	261	$\nu(\text{NN}), \nu_4$	62

<sup>a</sup>The functional groups, regions of maximum scattering, and vibrational modes are obtained from refs 53, 59, and 62–64. <sup>b</sup>The uncertainties are equal to, or less than, 1 cm<sup>-1</sup> unless stated otherwise. <sup>c</sup>Key:  $\nu$ , stretching;  $\delta$ , bending;  $r$ , rocking;  $\omega$ , wagging;  $s$ , symmetric;  $as$ , antisymmetric.

→  $\pi^*_{\text{CN}}$  transitions of the [B(CN)<sub>4</sub>]<sup>-</sup> anion. An  $n_{\text{N}}$  →  $\pi^*_{\text{CN}}$  transition cannot, however, explain the full range of the absorption structure observed here. After reaction with nitrogen dioxide, a second reflectance minimum appears in the range from approximately 300 to 600 nm. To help explain the cause of the broad new feature, the increase in the absorption was determined by subtracting the final reflectance spectrum from the unreacted reflectance spectrum, and the result is shown in

Figure 8b. The subtracted spectrum reveals a large, asymmetric absorption increase from 300 to 600 nm that reaches a maximum at around 440 nm. The UV–vis spectrum of [BMIM][DCA] after oxidation with nitrogen dioxide contains a relatively sharp absorption peak at 215 nm and two very broad structures with maxima at approximately 350 and 470 nm, and it was suggested that these peaks could have formed by nitrogen dioxide and dinitrogen tetroxide dissolving in the droplet.<sup>29</sup> In contrast, Figure 8b contains only a single peak and therefore cannot be fully accounted for by dissolved NO<sub>2</sub> or N<sub>2</sub>O<sub>4</sub>. The oxidation by nitrogen dioxide caused the absorption in the UV region to increase relative to that in the optical and near-infrared ranges and the absorption maximum to extend to longer wavelengths. It is well-established that conjugated  $\pi$ -electron systems involving double bonds absorb in the UV spectral region, and each additional double bond causes the absorption maxima for the  $\pi$  →  $\pi^*$  excitations to shift to longer wavelengths. The spectra in Figure 8 therefore suggest that oxidation produced an increase in the number of conjugated double bonds, which is likely consistent with polymerization.<sup>56</sup> Examples of relevant conjugated systems with absorption maxima near 440 nm are the conjugated organic nitro system 1,3,5-trinitrobenzene with aliphatic side chains, which has a maximum absorption in 450–456 nm region, and the boron-containing conjugated system, B-trimethyl-N-trimethylborazine, with a maximum absorption at 461 nm.<sup>57,58</sup>

**3.3. Reaction Mechanisms.** As discussed in section 3.2.1, the simplest reaction mechanism involves a nitrogen or oxygen atom of nitrogen dioxide attacking the [BMIM]<sup>+</sup> cation or [DCBH]<sup>-</sup> anion. Scheme 3 presents a summary of the reaction between nitrogen dioxide and [BMIM][DCBH] along with the formation of the functional groups depending on which ion the nitrogen dioxide molecule reacts with. The reaction between nitrogen dioxide and the [BMIM]<sup>+</sup> cation could lead to the formation of organic nitrites, aromatic nitro compounds, aliphatic nitro compounds, nitroamines, and carbonitrates functional groups. The addition of the nitrogen atom of nitrogen dioxide to the imidazolium ring would form the aromatic nitro compounds, while the addition of nitrogen dioxide to the butyl or methyl side chains would form the aliphatic nitro compounds. The organic nitrites are generated by the formation of a new bond between an oxygen atom of nitrogen dioxide to [BMIM]<sup>+</sup>. Lastly, the formation of carbonitrates occurs from the addition of the nitrogen atom to a carbon atom of the cation, while the addition of the nitrogen atom to a nitrogen atom of the cation would lead to the formation of nitroamines.

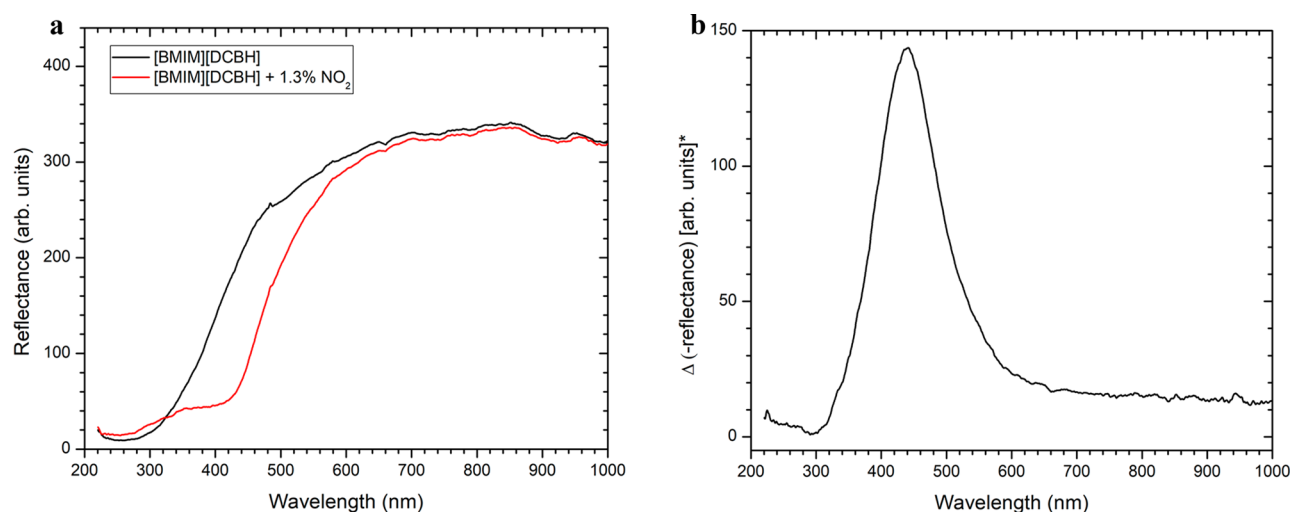
The nitrogen dioxide molecule can also react with three atoms in the [DCBH]<sup>-</sup>: boron, nitrogen, or carbon atoms. If the nitrogen dioxide attacks the boron atom in the anion, it could lead to the formation of B–N and B–O compounds. The nitrogen dioxide can also attack the carbon atom leading to the formation of nitrites, carbonitrates, or aliphatic nitro compounds. Lastly, the nitrogen dioxide can react with the nitrogen atom of the anion, leading to the formation of nitroamines (Scheme 3).

Overall, the FTIR spectra after the reaction in Figure 5 shows a noticeable decrease in the 1900–2600 cm<sup>-1</sup> wavenumber region which contains [DCBH]<sup>-</sup> fundamental modes, while the C–H vibrational modes of the [BMIM]<sup>+</sup> cation in the region of 2600–3400 cm<sup>-1</sup> appear unaffected. This suggests that the NO<sub>2</sub> prefers to attack the anion over the cation. This is consistent with our previous work on the oxidation of ionic liquids with

**Table 5.** Assignments of the New Peaks in the 532 nm Raman Spectra of [BMIM][DCBH] Levitated in 1.3% NO<sub>2</sub> and 98.7% Argon<sup>a</sup>

present wavenumbers (cm <sup>-1</sup> ) <sup>b</sup>	functional group/molecule	region (cm <sup>-1</sup> )	vibrational modes <sup>c</sup>	ref	present wavenumbers (cm <sup>-1</sup> ) <sup>b</sup>	functional group/molecule	region (cm <sup>-1</sup> )	vibrational modes <sup>c</sup>	ref
2235	NCO <sup>-</sup>	2250–2100	$\nu_1$	65	933 ± 3	aromatic nitro compounds	1180–865	$\nu(\text{CN})$	53
2092 ± 3–1954 ± 2 <sup>d</sup>	O=N–C=O	2045	$\nu(\text{CO})$	66	933 ± 3	aliphatic nitro compound	1000–915	$\nu(\text{CN})$	53
2092 ± 3–1954 ± 2 <sup>d</sup>	O=N–C=O	1969	$\nu_2 + \nu_4$	66	801	organic nitrites	815–750	$\nu(\text{N–O})$	53
2092 ± 3–1954 ± 2 <sup>d</sup>	O=N–N=C	1967	$\nu(\text{CN})$	62	801	N <sub>2</sub> O <sub>4</sub>	808	$\nu_2$	63
1897 ± 2	N=C=O	1921	$\nu_{\text{as}}(\text{NCO})$	55	801	unreacted [BMIM][DCBH]	811	see Table 2	
1865 ± 2	N–O–C≡N	1841	$\nu(\text{NO})$	67			789		
1833 ± 2	N–O–C≡N	1837	$\nu(\text{NO})$	62	640 ± 2	nitroamines	730–590	$\omega(\text{NO}_2)$	53
1833 ± 2	ONO–NO <sub>2</sub>	1825	$\nu(\text{N=O})$	68	642 ± 2	aliphatic nitro compounds	660–610	in-plane bend	60
1789 ± 6–1741 ± 8 <sup>d</sup>	N <sub>2</sub> O <sub>4</sub>	1791	$\nu_4 + \nu_5$	63	640 ± 2	unreacted [BMIM][DCBH]	657	see Table 2	
		1758	$\nu_9$				622		
1789 ± 6–1741 ± 8 <sup>d</sup>	O=N–C=O	1772	$\nu_2 + \nu_5$	66	490 ± 2	aliphatic nitro compounds	560–477	out-of-plane wag	60
1669–1611 ± 3 <sup>d</sup>	organic nitrites, <i>cis</i> form	1680–1650	$\nu(\text{N=O})$	53			495–470	in-plane rock	
1669–1611 ± 3 <sup>d</sup>	ONO–NO <sub>2</sub>	1656	$\nu_{\text{as}}(\text{NO}_2)$	68	490 ± 2	ONO–NO <sub>2</sub>	488	$\delta(\text{ONO})$	68
1669–1611 ± 3 <sup>d</sup>	nitroamines	1630–1530	$\nu_{\text{as}}(\text{NO}_2)$	53	490 ± 2	unreacted [BMIM][DCBH]	511	see Table 2	
1669–1611 ± 3 <sup>d</sup>	organic nitrites, <i>trans</i> forms	1625–1610	$\nu(\text{N=O})$	53					
1374 ± 2	covalent B–N compounds	1550–1330	$\nu(\text{B–N})$	53	416 ± 3	O=N–C≡N	411	$\nu_5 + \nu_6$	62
1374 ± 2	aliphatic nitro compounds	1381–1310	$\nu_s(\text{N=O})$	53	416 ± 3	unreacted [BMIM][DCBH]	417	see Table 2	
1374 ± 2	B–O	1380–1310	$\nu(\text{B–O})$	53					
1327	aliphatic nitro compounds	1381–1310	$\nu_s(\text{N=O})$	53					
1327	B–O	1380–1310	$\nu(\text{B–O})$	53					
1293	carbonitrates	1315–1205	$\nu_{\text{as}}(\text{NO}_2)$	53					
1293	nitroamines	1315–1260	$\nu_2(\text{NO}_2)$	53					
1293	ONO–NO <sub>2</sub>	1293	$\nu_1(\text{NO}_2)$	68					

<sup>a</sup>The functional groups, regions of maximum scattering, and vibrational modes are obtained from refs 53, 55, 62, 63, and 65–68. <sup>b</sup>The uncertainties are equal to, or less than, 1 cm<sup>-1</sup> unless stated otherwise. <sup>c</sup>Key:  $\nu$ , stretching;  $\delta$ , bending;  $\tau$ , rocking;  $\omega$ , wagging;  $\tau$ , torsion;  $s$ , symmetric;  $as$ , antisymmetric. <sup>d</sup>Broad, overlapping peaks that are better regarded as an unresolved combination of modes within the stated range.

**Figure 8.** UV–vis reflectance spectra for a droplet of (a) [BMIM][DCBH] before (black line) and after (red line) reaction with nitrogen dioxide and (b) the increase in the absorption calculated by subtracting the final reflectance spectrum from the unreacted reflectance spectrum.

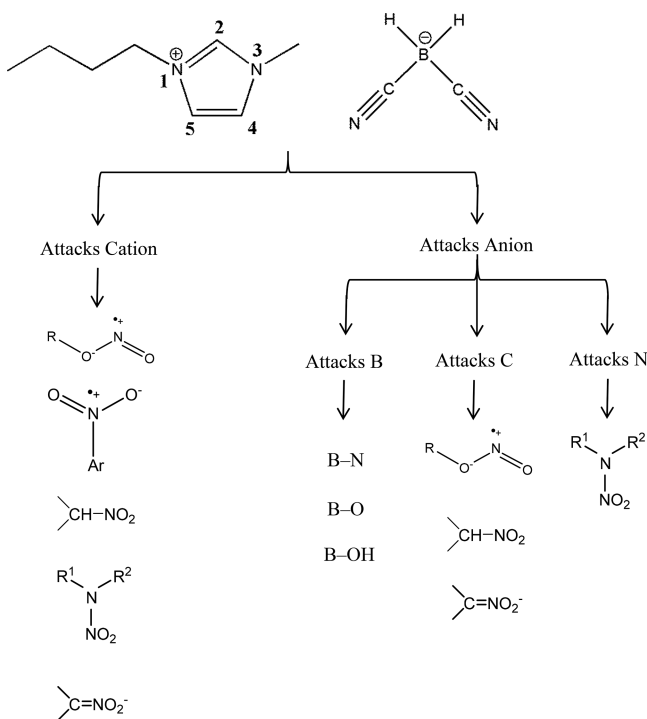
NO<sub>2</sub>.<sup>28,29,54</sup> The oxidations of ionic liquids are very complex systems, so further reactions may occur.

#### 4. CONCLUSION

The oxidation of a levitated [BMIM][DCBH] droplet by nitrogen dioxide was studied using FTIR, Raman, and UV–vis

spectroscopies. To determine the changes in the spectra due to the oxidation by nitrogen dioxide, the FTIR and Raman spectra were collected before the reaction, and the spectra were assigned for the first time. A [BMIM][DCBH] droplet was levitated in a gas mixture containing 1.3% NO<sub>2</sub> and 98.7% argon. Comparing the FTIR and Raman spectra before and after the oxidation

**Scheme 3. Schematic Summary of the Reaction Mechanism of Nitrogen Dioxide with [BMIM][DCBH] Leading to Distinct Functional Groups As Detected Spectroscopically**



revealed that numerous new peaks appeared. The spectra produced by oxidation of the ionic liquids are complex; therefore, FTIR and Raman spectroscopy alone cannot identify the specific molecules formed, but these techniques can be used to identify the possible functional groups of the reaction products. The simplest reaction mechanism would involve the nitrogen or oxygen atom of nitrogen dioxide bonding to one of the ions. The peak heights corresponding to the B–H and C–N fundamental stretching modes of the anion in the spectral region from 2000 to 2400  $\text{cm}^{-1}$  decreased by a factor of 2 following oxidation, whereas the C–H stretching region of the [BMIM]<sup>+</sup> cation in the range of 2600 to 3400  $\text{cm}^{-1}$  showed no significant change in intensity. Therefore, the spectra suggest that the nitrogen dioxide molecule is more likely to react with the [DCBH]<sup>−</sup> anion than the [BMIM]<sup>+</sup> cation. The assignment of large, new features in the oxidized spectra to B–N and B–O containing functional groups supports the suggestion that nitrogen dioxide reacts significantly with the anion. A reaction between nitrogen dioxide and the cation remains a possibility, however, subject to the requirement that the C–H stretching region of the [BMIM]<sup>+</sup> cation from 2600 to 3400  $\text{cm}^{-1}$  is unaffected. The oxidation by nitrogen dioxide caused the absorption in the UV region to increase relative to that in the optical and near-infrared ranges and the absorption maximum to extend to longer wavelengths, which suggest an increase in the number of conjugated double bonds and hence polymerization. Further theoretical and experimental studies are required to fully understand the complete reaction mechanisms.

It is informative to compare the present results with our previous studies on the oxidation by nitrogen dioxide of [MAT][DCA],<sup>28,29</sup> [BMIM][DCA],<sup>29</sup> and [AMIM][DCA].<sup>54</sup> The nitrogen dioxide was found to react significantly with both the [DCBH]<sup>−</sup> or [DCA]<sup>−</sup> anions. For all four ionic liquids, the new peaks are consistent with the formation of functional groups

of organic nitro-compounds, but only [BMIM][DCBH] formed structure produced by boron-containing compounds as expected. There also appears to be a difference in the oxidation of the boron when incorporated into the anion or added to the ionic liquid in the form of nanoparticles, as in the previous studies.<sup>28,29,54</sup> The vibrational spectra of [BMIM][DCBH] after oxidation showed evidence for oxidized boron such as the B–N and B–O vibrational modes. In contrast, the IL-capped boron nanoparticles produced only minor effects on the vibrational spectra of the [DCA]<sup>−</sup>-containing ILs, implying that the IL capping limited the oxidation of the nanoparticles.<sup>28,29,54</sup>

## ■ ASSOCIATED CONTENT

### 📄 Supporting Information

The Supporting Information is available free of charge on the ACS Publications website at DOI: 10.1021/acs.jpca.8b11796.

Analysis of 1-butyl-3-methylimidazolium dicyanoborate and description of analytical instruments (PDF)

## ■ AUTHOR INFORMATION

### Corresponding Author

\*E-mail: ralfk@hawaii.edu.

### ORCID

Maik Finze: 0000-0002-6098-7148

Ralf I. Kaiser: 0000-0002-7233-7206

### Notes

The authors declare no competing financial interest.

## ■ ACKNOWLEDGMENTS

This work was supported by the Office of Naval Research under Grant N00014-16-1-2078 (Hawaii).

## ■ REFERENCES

- (1) Clark, J. D. *Ignition! An Informal History of Liquid Rocket Propellants*; Rutgers University Press: New Brunswick, NJ, 1972.
- (2) Lei, Z.; Chen, B.; Koo, Y.-M.; MacFarlane, D. R. Introduction: Ionic Liquids. *Chem. Rev.* **2017**, *117*, 6633–6635.
- (3) Chand, D.; Zhang, J.; Shreeve, J. n. M. Borohydride Ionic Liquids as Hypergolic Fuels: A Quest for Improved Stability. *Chem. - Eur. J.* **2015**, *21*, 13297–13301.
- (4) Wang, K.; Zhang, Y.; Chand, D.; Parrish, D. A.; Shreeve, J. n. M. Boronium-Cation-Based Ionic Liquids as Hypergolic Fluids. *Chem. - Eur. J.* **2012**, *18*, 16931–16937.
- (5) Zhang, Q.; Shreeve, J. M. Energetic Ionic Liquids as Explosives and Propellant Fuels: A New Journey of Ionic Liquid Chemistry. *Chem. Rev.* **2014**, *114*, 10527–10574.
- (6) McCrary, P. D.; Chatel, G.; Alaniz, S. A.; Cojocaru, O. A.; Beasley, P. A.; Flores, L. A.; Kelley, S. P.; Barber, P. S.; Rogers, R. D. Evaluating Ionic Liquids as Hypergolic Fuels: Exploring Reactivity from Molecular Structure. *Energy Fuels* **2014**, *28*, 3460–3473.
- (7) Litzinger, T.; Iyer, S. Hypergolic Reaction of Dicyanamide-Based Fuels with Nitric Acid. *Energy Fuels* **2011**, *25* (1), 72–76.
- (8) Zhang, Q.; Shreeve, J. M. Ionic Liquid Propellants: Future Fuels for Space Propulsion. *Chem. - Eur. J.* **2013**, *19*, 15446–15451.
- (9) Zhang, Y.; Gao, H.; Joo, Y.-H.; Shreeve, J. M. Ionic Liquids as Hypergolic Fuels. *Angew. Chem., Int. Ed.* **2011**, *50*, 9554–9562.
- (10) Schneider, S.; Hawkins, T.; Rosander, M.; Vaghjiani, G.; Chambreau, S.; Drake, G. Ionic Liquids as Hypergolic Fuels. *Energy Fuels* **2008**, *22*, 2871–2872.
- (11) Chambreau, S. D.; Schneider, S.; Rosander, M.; Hawkins, T.; Gallegos, C. J.; Pastewait, M. F.; Vaghjiani, G. L. Fourier Transform Infrared Studies in Hypergolic Ignition of Ionic Liquids. *J. Phys. Chem. A* **2008**, *112*, 7816–7824.

- (12) Catoire, L.; Chambreau, S. D.; Vaghjiani, G. L. Chemical Kinetics Interpretation of Hypergolicity of Dicyanamide Ionic Liquid-Based Systems. *Combust. Flame* **2012**, *159*, 1759–1768.
- (13) Chambreau, S. D.; Koh, C. J.; Popolan-Vaida, D. M.; Gallegos, C. J.; Hooper, J. B.; Bedrov, D.; Vaghjiani, G. L.; Leone, S. R. Flow-Tube Investigations of Hypergolic Reactions of a Dicyanamide Ionic Liquid Via Tunable Vacuum Ultraviolet Aerosol Mass Spectrometry. *J. Phys. Chem. A* **2016**, *120*, 8011–8023.
- (14) Politzer, P.; Murray, J. S.; Seminario, J. M.; Lane, P.; Edward Grice, M.; Concha, M. C. Computational Characterization of Energetic Materials. *J. Mol. Struct.: THEOCHEM* **2001**, *573*, 1–10.
- (15) Rice, B. M.; Pai, S. V.; Hare, J. Predicting Heats of Formation of Energetic Materials using Quantum Mechanical Calculations. *Combust. Flame* **1999**, *118*, 445–458.
- (16) Cox, J. D.; Wagman, D. D.; Medvedev, V. A. *CODATA Key Values for Thermodynamics*; Hemisphere Publishing Corp.: New York, NY, 1989.
- (17) Ulas, A.; Kuo, K. K.; Gotzmer, C. Ignition and Combustion of Boron Particles in Fluorine-Containing Environments. *Combust. Flame* **2001**, *127*, 1935–1957.
- (18) Antaki, P.; Williams, F. A. Observations on the Combustion of Boron Slurry Droplets in Air. *Combust. Flame* **1987**, *67*, 1–8.
- (19) King, M. K. Ignition and Combustion of Boron Particles and Clouds. *J. Spacecr. Rockets* **1982**, *19*, 294–306.
- (20) Young, G.; Sullivan, K.; Zachariah, M. R.; Yu, K. Combustion Characteristics of Boron Nanoparticles. *Combust. Flame* **2009**, *156*, 322–333.
- (21) Zhou, W.; Yetter, R. A.; Dryer, F. L.; Rabitz, H.; Brown, R. C.; Kolb, C. E. Multi-Phase Model for Ignition and Combustion of Boron Particles. *Combust. Flame* **1999**, *117*, 227–243.
- (22) Perez, J. P. L.; McMahon, B. W.; Anderson, S. L. Functionalization and Passivation of Boron Nanoparticles with a Hypergolic Ionic Liquid. *J. Propul. Power* **2013**, *29*, 489–495.
- (23) L. Perez, J. P.; McMahon, B. W.; Schneider, S.; Boatz, J. A.; Hawkins, T. W.; McCrary, P. D.; Beasley, P. A.; Kelley, S. P.; Rogers, R. D.; Anderson, S. L. Exploring the Structure of Nitrogen-Rich Ionic Liquids and Their Binding to the Surface of Oxide-Free Boron Nanoparticles. *J. Phys. Chem. C* **2013**, *117*, 5693–5707.
- (24) Perez, J. P. L.; McMahon, B. W.; Yu, J.; Schneider, S.; Boatz, J. A.; Hawkins, T. W.; McCrary, P. D.; Flores, L. A.; Rogers, R. D.; Anderson, S. L. Boron Nanoparticles with High Hydrogen Loading: Mechanism for B-H Binding and Potential for Improved Combustibility and Specific Impulse. *ACS Appl. Mater. Interfaces* **2014**, *6*, 8513–8525.
- (25) Perez, J. P. L.; Yu, J.; Sheppard, A. J.; Chambreau, S. D.; Vaghjiani, G. L.; Anderson, S. L. Binding of Alkenes and Ionic Liquids to B-H-Functionalized Boron Nanoparticles: Creation of Particles with Controlled Dispersibility and Minimal Surface Oxidation. *ACS Appl. Mater. Interfaces* **2015**, *7*, 9991–10003.
- (26) McCrary, P. D.; Beasley, P. A.; Cojocar, O. A.; Schneider, S.; Hawkins, T. W.; Perez, J. P. L.; McMahon, B. W.; Pfeil, M.; Boatz, J. A.; Anderson, S. L.; et al. Hypergolic Ionic Liquids to Mill, Suspend, and Ignite Boron Nanoparticles. *Chem. Commun.* **2012**, *48*, 4311–4313.
- (27) Yu, J.; Jensen, T. N.; Lewis, W. K.; Bunker, C. E.; Kelley, S. P.; Rogers, R. D.; Pryor, O. M.; Chambreau, S. D.; Vaghjiani, G. L.; Anderson, S. L. Combustion Behavior of High Energy Density Borane-Aluminum Nanoparticles in Hypergolic Ionic Liquids. *Energy Fuels* **2018**, *32*, 7898–7908.
- (28) Brotton, S. J.; Lucas, M.; Chambreau, S. D.; Vaghjiani, G. L.; Yu, J.; Anderson, S. L.; Kaiser, R. I. Spectroscopic Investigation of the Primary Reaction Intermediates in the Oxidation of Levitated Droplets of Energetic Ionic Liquids. *J. Phys. Chem. Lett.* **2017**, *8*, 6053–6059.
- (29) Brotton, S. J.; Lucas, M.; Jensen, T. N.; Anderson, S. L.; Kaiser, R. I. Spectroscopic Study on the Intermediates and Reaction Rates in the Oxidation of Levitated Droplets of Energetic Ionic Liquids by Nitrogen Dioxide. *J. Phys. Chem. A* **2018**, *122*, 7351–7377.
- (30) Sebastiao, E.; Cook, C.; Hu, A.; Murugesu, M. Recent Developments in the Field of Energetic Ionic Liquids. *J. Mater. Chem. A* **2014**, *2*, 8153–8173.
- (31) Zhang, Y.; Shreeve, J. n. M. Dicyanoborate-Based Ionic Liquids as Hypergolic Fluids. *Angew. Chem., Int. Ed.* **2011**, *50*, 935–937.
- (32) Zhang, Y. Q.; Gao, H. X.; Joo, Y. H.; Shreeve, J. M. Ionic Liquids as Hypergolic Fuels. *Angew. Chem., Int. Ed.* **2011**, *50*, 9554–9562.
- (33) Brotton, S. J.; Kaiser, R. I. Novel High-Temperature and Pressure-Compatible Ultrasonic Levitator Apparatus Coupled to Raman and Fourier Transform Infrared Spectrometers. *Rev. Sci. Instrum.* **2013**, *84*, 055114.
- (34) Brotton, S. J.; Kaiser, R. I. In Situ Raman Spectroscopic Study of Gypsum ( $\text{CaSO}_4 \cdot 2\text{H}_2\text{O}$ ) and Epsomite ( $\text{MgSO}_4 \cdot 7\text{H}_2\text{O}$ ) Dehydration Utilizing an Ultrasonic Levitator. *J. Phys. Chem. Lett.* **2013**, *4*, 669–673.
- (35) Kerpen, C.; Sprenger, J. A. P.; Herkert, L.; Schäfer, M.; Bischoff, L. A.; Zeides, P.; Grüne, M.; Bertermann, R.; Brede, F. A.; Müller-Buschbaum, K.; et al. Protonation versus Oxonium Salt Formation: Basicity and Stability Tuning of Cyanoborate Anions. *Angew. Chem., Int. Ed.* **2017**, *56* (10), 2800–2804.
- (36) Bischoff, L. A.; Drisch, M.; Kerpen, C.; Hennig, P. T.; Landmann, J.; Sprenger, J. A. P.; Bertermann, R.; Grüne, M.; Yuan, Q.; Warneke, J.; Wang, X.; Ignat'ev, M.; Finze, M. Cyanohydroborate Anions: Synthesis, Salts, and Low-viscosity Ionic Liquids. *Chem. - Eur. J.* DOI: [10.1002/chem.201804698](https://doi.org/10.1002/chem.201804698). Ignatyev, N. M.; Sprenger, J. A. P.; Landmann, J.; Finze, M. *Method for Producing Salts having Hydridocyanoborate Anions*. U.S. Patent 2016/0130285 A1, 2016.
- (37) Kamemoto, L. E.; Misra, A. K.; Sharma, S. K.; Goodman, M. T.; Luk, H.; Dykes, A. C.; Acosta, T. Near-Infrared Micro-Raman Spectroscopy for In Vitro Detection of Cervical Cancer. *Appl. Spectrosc.* **2010**, *64*, 255–261.
- (38) Katsyuba, S. A.; Zvereva, E. E.; Vidis, A.; Dyson, P. J. Application of Density Functional Theory and Vibrational Spectroscopy Toward the Rational Design of Ionic Liquids. *J. Phys. Chem. A* **2007**, *111*, 352–370.
- (39) Spielvogel, B. F.; Ahmed, F. U.; Das, M. K.; McPhail, A. T. Synthesis of Sodium and Tetra-n-butylammonium Dicyanodihydroborate. *Inorg. Chem.* **1984**, *23*, 3263–3265.
- (40) Berschied, J. R., Jr.; Purcell, K. F. Spectroscopic and Chemical Properties of the Cyanotrihydroborate Anion. *Inorg. Chem.* **1970**, *9*, 624–629.
- (41) Scheers, J.; Johansson, P.; Jacobsson, P. Anions for Lithium Battery Electrolytes: A Spectroscopic and Theoretical Study of the  $\text{B}(\text{CN})_4^-$  Anion of the Ionic Liquid  $\text{C}_2\text{mim}[\text{B}(\text{CN})_4]$ . *J. Electrochem. Soc.* **2008**, *155*, A628–A634.
- (42) Paschoal, V. H.; Faria, L. F. O.; Ribeiro, M. C. C. Vibrational Spectroscopy of Ionic Liquids. *Chem. Rev.* **2017**, *117*, 7053–7112.
- (43) Holomb, R.; Martinelli, A.; Albinsson, I.; Lassegues, J. C.; Johansson, P.; Jacobsson, P. Ionic Liquid Structure: The Conformational Isomerism in 1-Butyl-3-methylimidazolium Tetrafluoroborate ( $[\text{BMIM}][\text{BF}_4]$ ). *J. Raman Spectrosc.* **2008**, *39*, 793–805.
- (44) Berg, R. W. Raman Spectroscopy and Ab-Initio Model Calculations on Ionic Liquids. *Monatsh. Chem.* **2007**, *138*, 1045–1075.
- (45) Heimer, N. E.; Del Sesto, R. E.; Meng, Z.; Wilkes, J. S.; Carper, W. R. Vibrational Spectra of Imidazolium Tetrafluoroborate Ionic Liquids. *J. Mol. Liq.* **2006**, *124*, 84–95.
- (46) Talaty, E. R.; Raja, S.; Storhaug, V. J.; Doelle, A.; Carper, W. R. Raman and Infrared Spectra and Ab Initio Calculations of  $\text{C}_{2-4}\text{MIM}$  Imidazolium Hexafluorophosphate Ionic Liquids. *J. Phys. Chem. B* **2004**, *108*, 13177–13184.
- (47) Scheers, J.; Pitawala, J.; Thebault, F.; Kim, J.-K.; Ahn, J.-H.; Matic, A.; Johansson, P.; Jacobsson, P. Ionic Liquids and Oligomer Electrolytes Based on the  $\text{B}(\text{CN})_4^-$  Anion; Ion Association, Physical and Electrochemical Properties. *Phys. Chem. Chem. Phys.* **2011**, *13*, 14953–14959.
- (48) Penalber, C. Y.; Baker, G. A.; Baldelli, S. Sum Frequency Generation Spectroscopy of Imidazolium-Based Ionic Liquids with Cyano-Functionalized Anions at the Solid Salt-Liquid Interface. *J. Phys. Chem. B* **2013**, *117*, 5939–5949.
- (49) Penalber, C. Y.; Grenoble, Z.; Baker, G. A.; Baldelli, S. Surface Characterization of Imidazolium-based Ionic Liquids with Cyano-functionalized Anions at the Gas-Liquid Interface using Sum Frequency

Generation Spectroscopy. *Phys. Chem. Chem. Phys.* **2012**, *14*, 5122–5131.

(50) Mao, J. X.; Lee, A. S.; Kitchin, J. R.; Nulwala, H. B.; Luebke, D. R.; Damodaran, K. Interactions in 1-Ethyl-3-methyl Imidazolium Tetracyanoborate Ion Pair: Spectroscopic and Density Functional Study. *J. Mol. Struct.* **2013**, *1038*, 12–18.

(51) Bernhardt, E.; Henkel, G.; Willner, H. The Tetracyanoborates  $M[B(CN)_4]$ ,  $M = [Bu_4N]^+$ ,  $Ag^+$ ,  $K^+$ . *Z. Anorg. Allg. Chem.* **2000**, *626*, 560–568.

(52) Koppers, T.; Bernhardt, E.; Willner, H.; Rohm, H. W.; Koeckerling, M. Tetracyanoborate Salts  $M[B(CN)_4]$  with  $M =$  Singly Charged Cations: Properties and Structures. *Inorg. Chem.* **2005**, *44*, 1015–1022.

(53) Socrates, G. *Infrared and Raman Characteristic Group Frequencies: Tables and Charts*, 3rd ed.; Wiley: New York, 2001; p xv.

(54) Lucas, M.; Brotton, S. J.; Shukla, S. K.; Yu, J.; Anderson, S. L.; Kaiser, R. I. Oxidation of a Levitated Droplet of 1-Allyl-3-Methylimidazolium Dicyanamide by Nitrogen Dioxide. *J. Phys. Chem. A* **2018**, DOI: 10.1021/acs.jpca.8b08395.

(55) Linstrom, P. J.; Mallard, W. G. *NIST Chemistry WebBook, Standard Reference Database Number 69*; National Institute of Standards and Technology: Gaithersburg, MD (<http://webbook.nist.gov>).

(56) Chingin, K.; Perry, R. H.; Chambreau, S. D.; Vaghjiani, G. L.; Zare, R. N. Generation of Melamine Polymer Condensates upon Hypersonic Ignition of Dicyanamide Ionic Liquids. *Angew. Chem., Int. Ed.* **2011**, *50*, 8634–8637.

(57) Fyfe, C. A. Interaction between Aliphatic and Aromatic Nitro Compounds in Basic Media. *Can. J. Chem.* **1968**, *46*, 3047–3054.

(58) Champion, N. G. S.; Foster, R.; Mackie, R. K.  $\pi$ -Molecular Complex of Hexamethylborazole with Tetracyanoethylene. *J. Chem. Soc.* **1961**, 5060.

(59) Bellamy, L. J.; Gerrard, W.; Lappert, M. F.; Williams, R. L. Infrared Spectra of Boron Compounds. *J. Chem. Soc.* **1958**, 2412–2415.

(60) Mayo, D. W.; Miller, F. A.; Hannah, R. W. *Course Notes on the Interpretation of Infrared and Raman Spectra*; John Wiley & Sons: New York, 2004.

(61) Smith, B. C. *Infrared Spectral Interpretation: A Systematic Approach*; CRC press: New York, 1998.

(62) Maier, G.; Reisenauer, H. P.; Eckwert, J.; Naumann, M.; De Marco, M. Isomers of the Elemental Composition  $CN_2O$ . *Angew. Chem., Int. Ed. Engl.* **1997**, *36*, 1707–1709.

(63) Bibart, C.; Ewing, G. Vibrational Spectrum, Torsional Potential, and Bonding of Gaseous  $N_2O_4$ . *J. Chem. Phys.* **1974**, *61*, 1284–1292.

(64) Nicolaisen, F. M.; Nielsen, O. J. Far Infrared Gas Spectra of Nitrosyl Cyanide. *J. Mol. Struct.* **1978**, *49*, 97–104.

(65) Nakamoto, K. *Infrared and Raman Spectra of Inorganic and Coordination Compounds*, 5th ed.; John Wiley & Sons, Inc.: New York, 1997.

(66) Wu, Y.-J.; Lee, Y.-P. Isomers of  $NCO_2$ : IR-Absorption Spectra of ONCO in Solid Ne. *J. Chem. Phys.* **2005**, *123*, 174301.

(67) Thompson, W. E.; Jacox, M. E. The Infrared Spectrum of  $NN\cdots CO^+$  Trapped in Solid Neon. *J. Chem. Phys.* **2011**, *135*, 224307.

(68) Beckers, H.; Zeng, X.; Willner, H. Intermediates Involved in the Oxidation of Nitrogen Monoxide: Photochemistry of the  $cis-N_2O_2 \cdot O_2$  complex and of  $sym-N_2O_4$  in Solid Ne Matrixes. *Chem. - Eur. J.* **2010**, *16*, 1506–1520.